Neuron

Co-packaging of opposing neurotransmitters in individual synaptic vesicles in the central nervous system

Graphical abstract

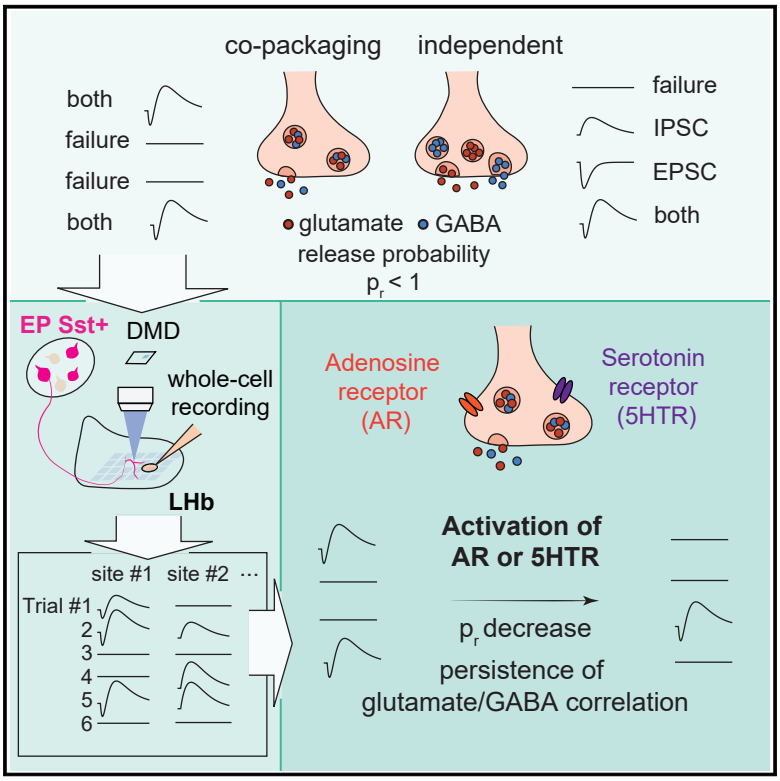

Highlights

- Different modes of synaptic co-release are computationally modeled and simulated
- A new method allows repeated analysis of individual synapses formed onto 1 neuron
- Individual synaptic vesicles of EP *Sst*+ boutons in LHb contain glutamate and GABA
- Co-release of glutamate/GABA results in correlated activation of AMPAR and $GABA_AR$

Authors

SeulAh Kim, Michael L. Wallace, Mahmoud El-Rifai, Alexa R. Knudsen, Bernardo L. Sabatini

Correspondence

bsabatini@hms.harvard.edu

In brief

Somatostatin-expressing entopedunculus projections to the lateral habenula release glutamate and GABA. Using mathematical simulations and new electrophysiological approaches, Kim et al. show that both neurotransmitters are packaged into the same synaptic vesicles. Inhibitors of release, such as serotonin, affect both transmitters by reducing probability of release of these co-packaged vesicles.

Kim et al., 2022, Neuron *110*, 1–14
April 20, 2022
https://doi.org/10.1016/j.neuron.2022.01.007

CellPress

Neuron

CellPress

Article

Co-packaging of opposing neurotransmitters in individual synaptic vesicles in the central nervous system

SeulAh Kim,[1] Michael L. Wallace,[1,3] Mahmoud El-Rifai,[2] Alexa R. Knudsen,[1] and Bernardo L. Sabatini[1,4,*]
[1]Howard Hughes Medical Institute, Department of Neurobiology, Harvard Medical School, 220 Longwood Ave, Boston, MA 02115, USA
[2]Department of Neurobiology, Harvard Medical School, 220 Longwood Ave, Boston, MA 01225, USA
[3]Present address: Department of Anatomy and Neurobiology, Boston University School of Medicine, 72 E. Concord St., Boston, MA 02118, USA
[4]Lead contact
*Correspondence: bsabatini@hms.harvard.edu
https://doi.org/10.1016/j.neuron.2022.01.007

SUMMARY

Many mammalian neurons release multiple neurotransmitters to activate diverse classes of postsynaptic ionotropic receptors. Entopeduncular nucleus somatostatin (EP *Sst*+) projection neurons to the lateral habenula (LHb) release both glutamate and GABA, but it is unclear whether these are packaged into the same or segregated pools of synaptic vesicles. Here, we describe a method combining electrophysiology, spatially patterned optogenetics, and computational modeling designed to analyze the mechanism of glutamate/GABA co-release in mouse brain. We find that the properties of postsynaptic currents elicited in LHb neurons by optogenetically activating EP *Sst*+ terminals are only consistent with co-packaging of glutamate/GABA into individual vesicles. Furthermore, presynaptic neuromodulators that weaken EP *Sst*+ to LHb synapses maintain the co-packaging of glutamate/GABA while reducing vesicular release probability. Our approach is applicable to the study of multi-transmitter neurons throughout the brain, and our results constrain the mechanisms of neuromodulation and synaptic integration in LHb.

INTRODUCTION

Many neurons in the mammalian brain produce, store, and release multiple neurotransmitters (Tritsch et al., 2016). Despite the prevalence of multi-transmitter neurons, our understanding of how, when, and where multiple neurotransmitters are released and what purpose co-release serves remains incomplete. At some multi-transmitter synapses, multiple small molecules (i.e., non-peptide) are packaged into the same vesicle (Jonas et al., 1998; Shabel et al., 2014; Tritsch et al., 2012), whereas in other cases a cell makes multiple classes of presynaptic boutons, each releasing a different transmitter (Granger et al., 2020; Lee et al., 2010; Zhang et al., 2015). Furthermore, even if two transmitters are released in the same vesicle from a single synaptic bouton, the opposing postsynaptic target may not have receptors for both, preventing co-transmission. Conversely, two transmitters may be released from different terminals, but if these form synapses onto the same cell, co-transmission will occur. For these reasons, the mechanisms of co-release at synapses formed by multi-transmitter neurons are difficult to determine from the average synaptic responses, necessitating experiments examining single release events from individual synapses.

Co-transmitting neurons are found in the entopeduncular nucleus (EP), a basal ganglia nucleus comprising multiple neural populations. Among these, somatostatin positive (*Sst*+) EP neurons project to the lateral habenula (LHb) and express the molecular machinery necessary to release glutamate and GABA (Wallace et al., 2017). Stimulation of EP *Sst*+ axons causes glutamate/GABA co-release and generates compound synaptic currents in LHb neurons, mediated by the opening of ionotropic glutamate and GABA receptors (Root et al., 2018; Wallace et al., 2017). At this synapse, glutamate and GABA may be packaged into the same vesicles, as supported by the detection of biphasic miniature spontaneous synaptic responses in LHb neurons (Shabel et al., 2014). Alternatively, they may be segregated in different pools of synaptic vesicles that are independently released from the same terminal, as supported by ultrastructural and biochemical evidence that glutamate and GABA vesicular transporters are found in separate pools of vesicles in LHb (Root et al., 2018).

The mechanism of glutamate/GABA co-release, and how it may be modulated by plasticity, will impact our understanding of EP-to-LHb circuit in the context of altered behavioral states. LHb regulates major monoaminergic centers in the brain (Hu et al., 2020; Matsumoto and Hikosaka, 2009,

Please cite this article in press as: Kim et al., Co-packaging of opposing neurotransmitters in individual synaptic vesicles in the central nervous system, Neuron (2022), https://doi.org/10.1016/j.neuron.2022.01.007

2007), and the EP is implicated in aversion, encoding of reward prediction error and action-outcome evaluation (Hong and Hikosaka, 2008; Li et al., 2019; Shabel et al., 2012; Stephenson-Jones et al., 2016). Furthermore, synaptic plasticity that shifts the relative proportion of glutamate/GABA co-transmission from EP to LHb alters the excitability (Li et al., 2011) and bursting states of LHb neurons (Yang et al., 2018). This change is believed to drive animals toward maladaptive behavior states, such as depression, chronic-stress-induced passive coping, and addiction (Cerniauskas et al., 2019; Li et al., 2011; Maroteaux and Mameli, 2012; Meye et al., 2016; Shabel et al., 2014; Trusel et al., 2019).

Here, we combine molecular, computational, pharmacological, and electrophysiological analyses to determine whether glutamate/GABA co-released at synapses between EP *Sst*+ and LHb neurons are packaged into the same or different synaptic vesicles. Immunohistochemical analysis of the distributions of synaptic proteins reveals that the proteins necessary for glutamate and GABA release are colocalized within individual EP *Sst*+ terminals. We characterize differential statistical features expected by the two distinct release modes and compare them with the experimental results collected, using an optogenetic approach that activates individual EP *Sst*+ boutons. We discover that glutamate and GABA are co-packaged into the same vesicles in EP *Sst*+ terminals. In addition, serotonin (5-HT) and adenosine each reduce the release probability of both transmitters while maintaining the correlation between glutamatergic and GABAergic unitary responses, further supporting that the two transmitters are released in the same vesicles.

RESULTS

Functional and molecular evidence of co-release from EP *Sst*+ axons in LHb

To gain optogenetic control over EP *Sst*+ cells, we bilaterally injected adeno-associated virus (AAV) that expresses the channelrhodopsin variant oChIEF in a Cre-dependent manner into the EP of *Sst-IRES-Cre* (*Sst-Cre*) mice (Figure 1A) (Lin et al., 2009; Taniguchi et al., 2011; Wallace et al., 2017). Optogenetic activation of EP *Sst*+ axons in brain slices triggered a biphasic postsynaptic current (PSC) in voltage-clamped LHb neurons (holding voltage, V_h = −35 mV) in the presence of NMDA receptor antagonist (CPP; Figure 1B). This current profile results from the faster channel kinetics of AMPA receptors (AMPARs) relative to $GABA_A$ receptors ($GABA_A$Rs). GABAergic and glutamatergic PSCs persist in the presence of TTX/4-AP, confirming direct release of both transmitters from the terminals (Wallace et al., 2017).

Individual EP *Sst*+ neurons express genes required for co-transmission (Root et al., 2018; Shabel et al., 2014; Wallace et al., 2017). To examine whether individual EP *Sst*+ boutons express the proteins required for release of both transmitters, we used array tomography (Micheva and Smith, 2007). Cre-dependent expression of synaptophysin-YFP induced by AAV injection into EP labeled *Sst*+ boutons in LHb. Serial sections were immunolabeled for YFP, Synapsin-1, Vglut2, Vgat, PSD95, and gephyrin (Figures 1C and 1D).

The presynaptic protein synapsin-1 was found within the YFP+ regions far more often than expected by chance (Figures 1E and S1B). Similarly, Vgat and Vglut2 puncta often overlapped (Figure 1D), with both found in YFP+ terminals far above chance (Figures 1E and S1C). We also found strong non-random overlap of gephyrin and weak, but still above-chance, overlap of PSD95 puncta with YFP+ boutons (Figures 1D, 1E, and S1C).

Whole-image analysis revealed weak cross-correlations across channels (mean: 0.003–0.294; individual: 0.0007–0.423) (Figure 1F), peaking at 0-pixel image displacement. Restricting analysis to the image areas within YFP-labeled terminals (n = 8,493; mean ∼0.3% of the image pixels; 4 tissue stacks, 3 animals) (Figure 1G) revealed high positive covariance of Vgat-Vglut2 signals, indicating overlap of glutamate and GABA vesicular transporters in EP *Sst*+ boutons. Similarly, analyzed Vgat-Gephyrin signals had high positive covariance, consistent with overlap of inhibitory pre- and postsynaptic densities for GABAergic terminals (Figures 1F and 1G). PSD95 signal did not exhibit positive covariance with other antibodies, possibly due to its low enrichment within the YFP+ boutons (Figures 1E and 1G) (Granger et al., 2020; Saunders et al., 2015). Thus, individual EP *Sst*+ presynaptic boutons in the LHb have the molecular machinery necessary to release both glutamate and GABA and colocalize with GABA receptors-associated scaffolding proteins.

Statistical features of PSCs generated by two models of co-release

We considered two models of glutamate/GABA co-release in LHb: one in which the two neurotransmitters are packaged in separate vesicles released from the same terminal (Root et al., 2018) (the "independent" model) and the other in which transmitters are packaged and released in the same vesicles (Shabel et al., 2014) (the "co-packaging" model) (Figure 2A). The PSCs produced by release under both models can appear identical when averaged across multiple stimuli of a single bouton or pooled across many co-active boutons. However, trial-by-trial analyses of PSCs resulting from stimulation of individual co-transmitting boutons differ in each model when vesicle release is stochastic (i.e., release probability, p_r, < 1) (Figures 2A and 2B).

We simulated PSCs generated by stochastic synaptic vesicle release under the independent and co-packaging models and computed three statistical features from the simulated datasets that quantify the qualitative differences evident in scatterplots of the maximum and minimum amplitudes of PSCs generated under the two models (Figure 2C). These features rely, at a varying level, on the ability to accurately detect the presence of an excitatory (EPSC) or inhibitory (IPSC) PSC in each trial (i.e., to distinguish successes from failures). Below, the maximum (i_{max}) and minimum (i_{min}) currents during a defined time window refer to amplitudes measured without judging whether a release event has occurred (i.e., they may be due to noise). In contrast, IPSC and EPSC and their amplitudes refer to the components of PSCs that were judged to be a success of GABA or glutamate release, respectively (i.e., the excitatory or inhibitory component rises out of the noise).

Please cite this article in press as: Kim et al., Co-packaging of opposing neurotransmitters in individual synaptic vesicles in the central nervous system, Neuron (2022), https://doi.org/10.1016/j.neuron.2022.01.007

CellPress

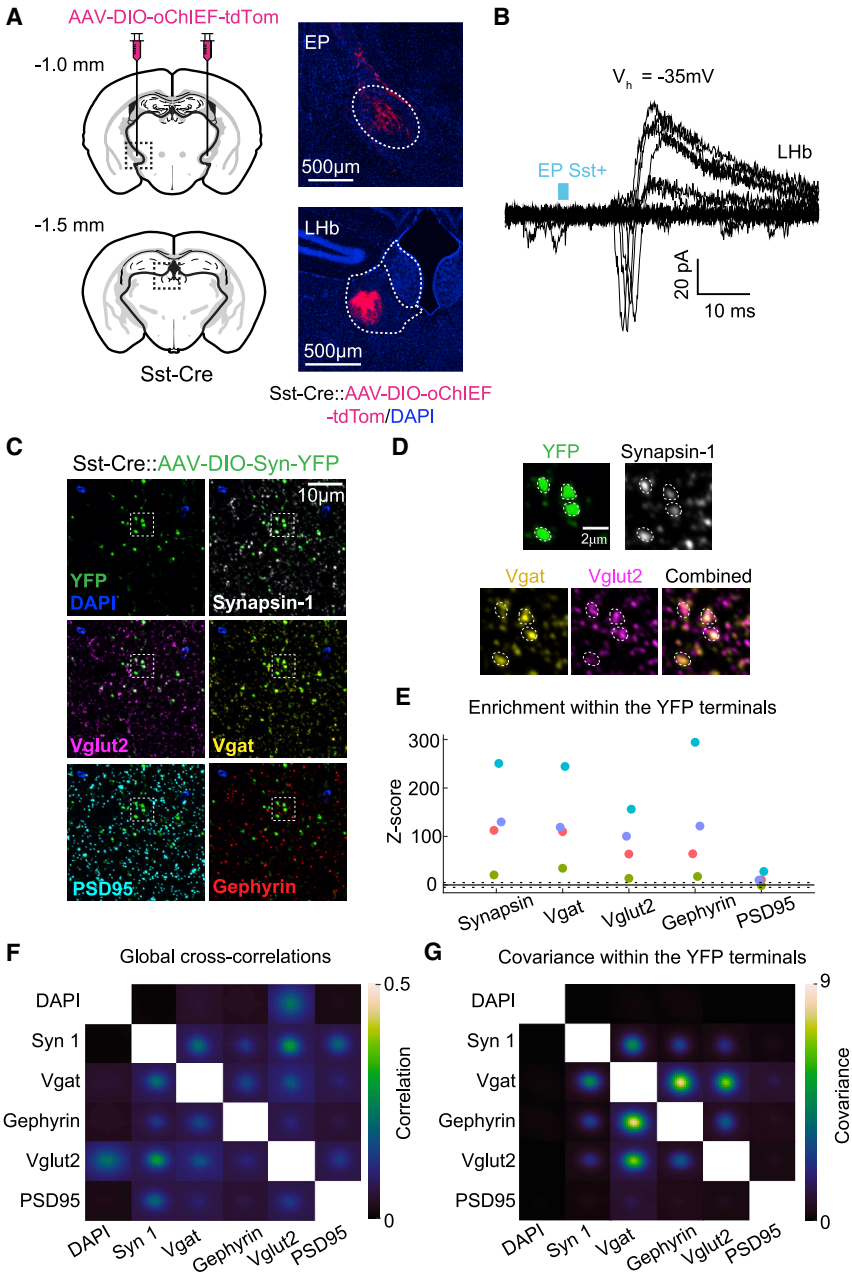

Figure 1. Electrophysiological and molecular evidence for glutamate/GABA co-release from EP *Sst*+ axons in LHb

(A) Left, injection of Cre-dependent AAV encoding the optogenetic activator oChIEF into the EP of *Sst-Cre* mice. Right, expression of tdTom in soma at the injection site (top) and in axons of EP *Sst*+ neurons in the LHb (bottom). Scale bars, 500 μm.

(B) PSCs recorded from a LHb neuron (V_h = −35 mV) following optogenetic activation of EP *Sst*+ axons using minimal stimulation in an acute brain slice. Some trials result in failures, whereas others evoke both inward and outward PSCs as seen in the biphasic PSCs. Blue: timing and duration of the laser pulse.

(C) Serial sections of brain tissue containing EP *Sst*+ terminals expressing synaptophysin-YFP were sequentially immunostained for multiplex fluorescence imaging. Field of view with antibodies against the pre- (synapsin 1 [white], Vglut2 [magenta], and Vgat [yellow]) and post- (PSD95 [cyan], gephyrin [red]) synaptic markers.

(D) Enlargement of the inset in (C) demonstrating colocalization in synapsin-1-expressing YFP-labeled *Sst*+ terminals (top) of proteins necessary for GABA (Vgat) and glutamate (Vglut2) release (bottom).

(E) *Z*-scored enrichment of immunopuncta within YFP+ boutons relative to that expected at random. Colors indicate data from the same image stack. Dashed lines: ±5 *Z* scores.

(F) Average cross-correlations of *Z*-scored fluorescence signals for all pairs of antibodies.

(G) Average co-variances of *Z*-scored fluorescence signals for all pairs of antibodies within the YFP+ terminals.

First, we considered the probabilities of detecting PSCs with different components and tested whether

$$p(E \cap I) = p(E)p(I) \quad \text{(Equation 1)}$$

in which p(E), p(I), and p(E∩I) are the measured probabilities of detecting an EPSC, IPSC, and compound PSC, respectively (Figure 2D). As expected, only independent release generated a distribution of joint probabilities that matched the distribution of the products of the individual probabilities (Figure 2D). Second, we compared the cumulative distribution functions (cdfs) of i_{max} and i_{min} in trials grouped by the presence and absence of EPSCs ("E" versus "no E") and IPSCs ("I" versus "no I") (Figure 2E). Only the co-packaging model is consistent with the presence or absence of one current fully predicting the presence or absence of the other current (Figure 2E). Although this assay requires detecting the presence of either the EPSC or the IPSC on each trial, it is robust to some errors in the accuracy of detection (Figure S2A). Third, we examined the trial-to-trial correlation of i_{max} and $-i_{min}$ (Figure 2F). In the independent model, i_{max} and $-i_{min}$ are negatively correlated (Figure 2F) as a large EPSC will reduce the size of an independently generated IPSC and vice versa. The co-packaging model produces strong positive correlations (~1) (Figure 2F) as a result of the co-occurrence of successes and failures in EPSCs/IPSCs and their shared variance due to vesicle-to-vesicle size differences.

DMD-based optogenetic stimulation to study co-release from EP *Sst*+ axons

Experimentally testing the predictions of the models required a method to record minimal responses from individual synapses in many trials. Thus, we implemented a digital micromirror device

Please cite this article in press as: Kim et al., Co-packaging of opposing neurotransmitters in individual synaptic vesicles in the central nervous system, Neuron (2022), https://doi.org/10.1016/j.neuron.2022.01.007

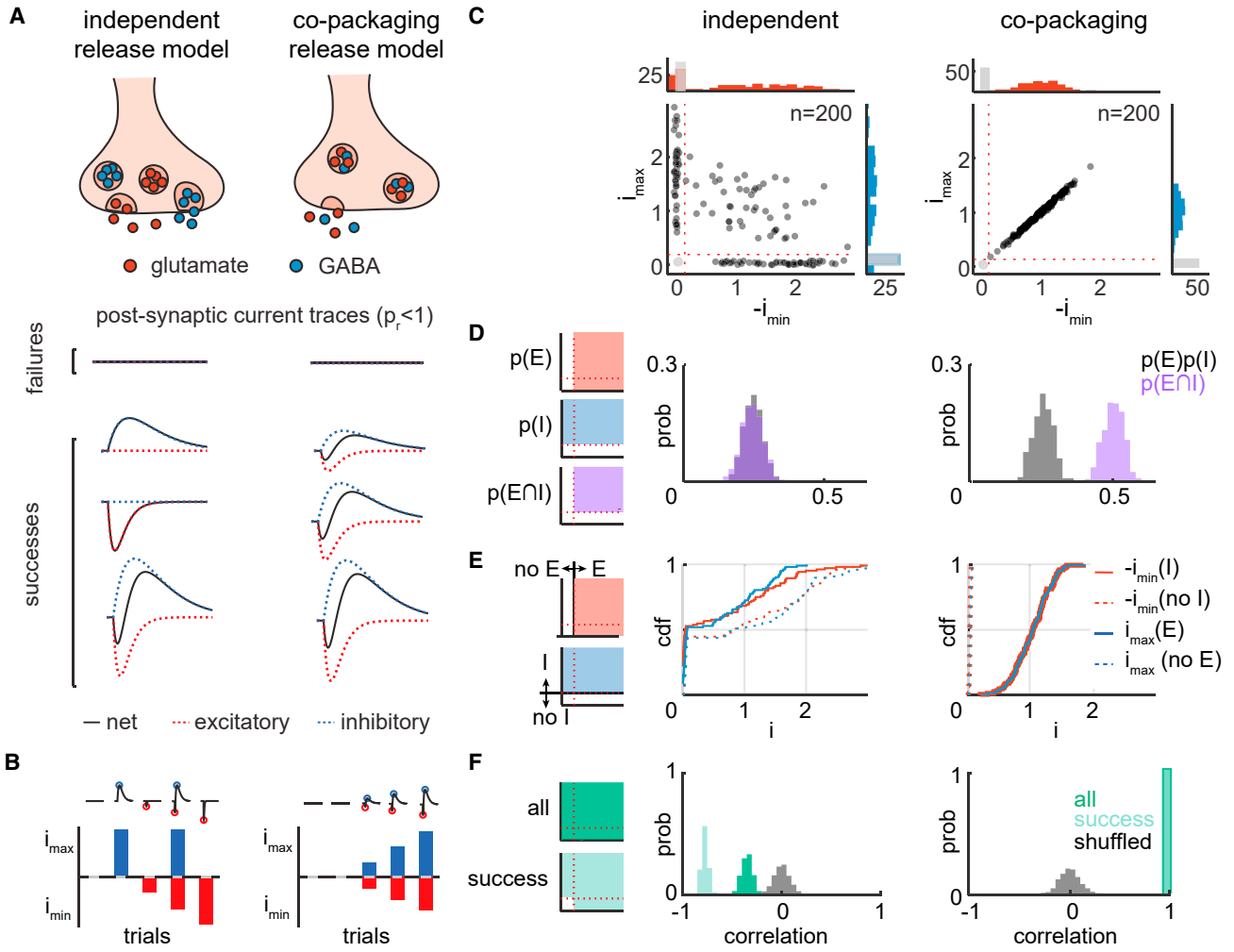

Figure 2. Statistical features of PSCs predicted by two models of co-release

(A) Top, potential modes of glutamate and GABA co-release from individual synaptic terminals in which each class of vesicle is released independently (left) or the neurotransmitters are co-packaged and released together in the same vesicle (right). Bottom, PSCs predicted by the independent (left) and co-packaging (right) models at low p_r.

(B) i_{max} and i_{min} for trials in (A) for the independent (left) and co-packaging (right) models.

(C) Scatterplots of i_{max} and $-i_{min}$ of 200 PSCs generated by simulations of independent ($p_r = 0.5$, left) and co-packaging ($p_r = 0.75$, right) models with the same rate of synaptic failures (0.25). Amplitudes are normalized to the average i_{max} (y axis) and $-i_{min}$ (x axis) of success trials. Histograms (in counts) of the normalized i_{max} and $-i_{min}$ with successes of release shown on the right (blue) and top (red) and failures of release in each shown in gray. Successes of release (i_{max} or $-i_{min}$ exceeds the thresholds indicated by red dotted lines) trials are shown by black filled circles whereas failures are in gray.

(D) Left, schematics of the areas within the scatterplots used to count events and calculate the probabilities of detecting inhibitory (p(I)) or excitatory (p(E)) currents as well as of biphasic currents (p(E∩I)). Center and right, the statistical independence of the probabilities of detecting inhibitory (p(I)) and excitatory (p(E)) PSCs for the two models; the observed probability of excitatory and inhibitory PSCs (p(E∩I), purple) was compared with that expected by chance (p(E)p(I), gray). Results for independent (center) and co-packaging (right) models are shown with $p_r = 0.5$ and were used in (E) and (F) as well.

(E) Left, schematics of the areas within the scatterplots used to determine presence or absence of excitatory (top) and inhibitory (bottom) PSCs in each trial. Center and right, simulated cdfs of i_{max} (blue) given the presence (i_{max}(E), solid) or absence (i_{max}(no E), dashed) of EPSC in the independent (center) and co-packaging (right) models. Similar analyses were performed for the $-i_{min}$ (red) given the presence ($-i_{min}$(I), solid) or absence ($-i_{min}$(no I), dashed) of an IPSC.

(F) Left, schematics of the areas of the scatterplots that contain all (top) or success (bottom) trials. Center and right, analysis of the trial-by-trial correlation of i_{max} and $-i_{min}$ of all trials (dark green), success trials (light green), and after shuffling (gray).

(DMD)-based optogenetic stimulation approach to activate co-releasing EP *Sst*+ boutons in the LHb (Figure 3A). Variants of this approach have been used to map connectivity and the spatial arrangement of cortical synapses (Petreanu et al., 2009, 2007).

We first examined DMD-evoked responses at high laser powers that activate many EP to LHb *Sst*+ boutons in brain slices (Figure 3B). LHb neurons were voltage-clamped at −70 and 0 mV, respectively, to record EPSCs and IPSCs (Figure 3C). In each neuron, a subset of the stimulation spots (252/576, 6 cells,

Please cite this article in press as: Kim et al., Co-packaging of opposing neurotransmitters in individual synaptic vesicles in the central nervous system, Neuron (2022), https://doi.org/10.1016/j.neuron.2022.01.007

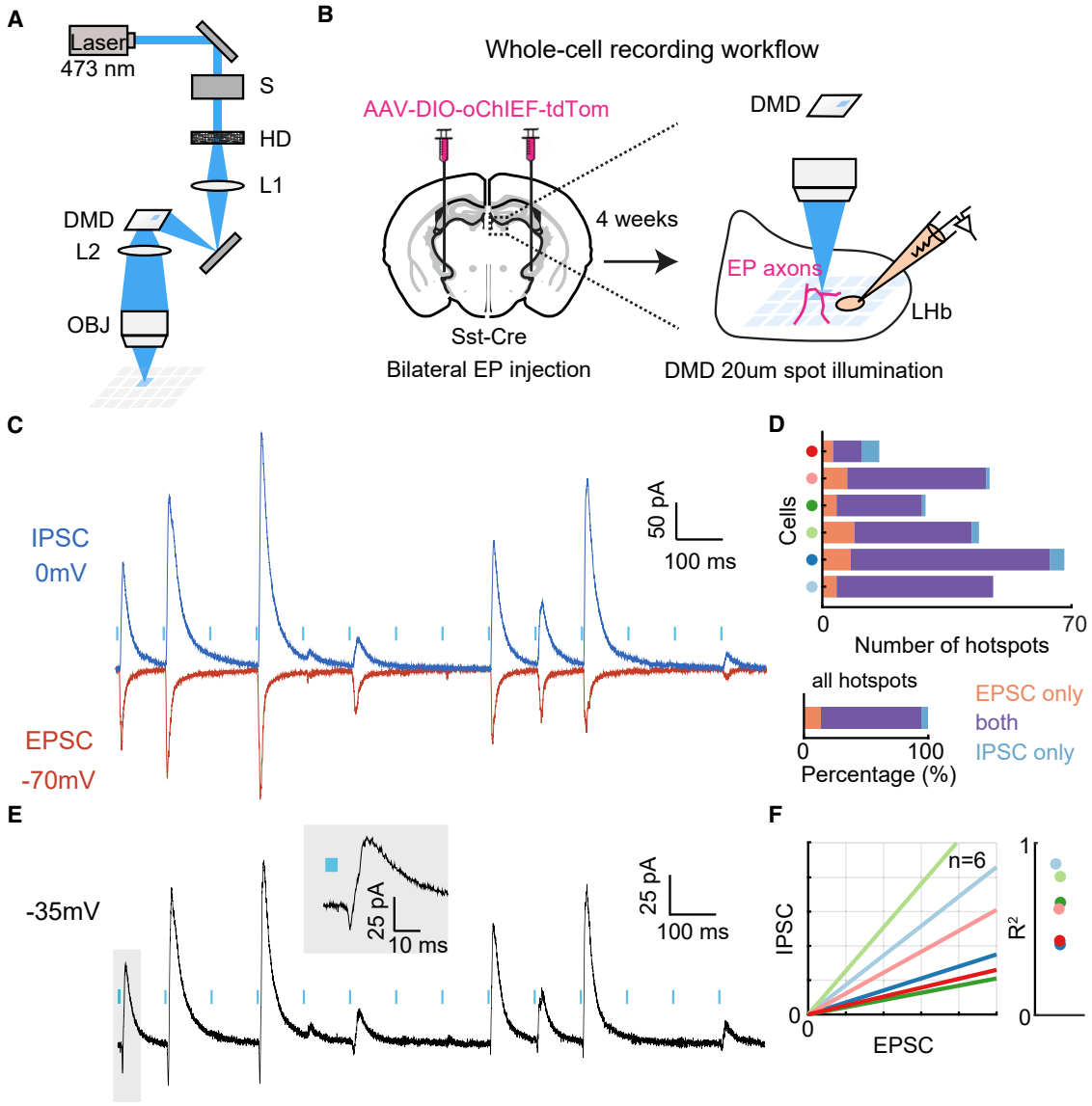

Figure 3. Approach to measure PSCs evoked by optogenetic stimulation of EP *Sst*+ axons in LHb

(A) DMOS setup. S, mechanical shutter; HD, holographic diffuser (10° diffusing angle); DMD, digital micromirror device; L1-2, lens; OBJ, objective lens.

(B) Workflow schematic of Cre-dependent AAV encoding the optogenetic activator oChIEF injection into the EP of *Sst-Cre* mice, followed by recordings in acute brain slices of LHb.

(C) Optically evoked average E- and IPSCs acquired at V_h = −70 (red) or 0 (dark blue) mV, respectively. Light blue vertical bars: timing of the laser stimulation pulses with each delivered to a different location in the slice. PSCs are the average of five trials.

(D) The number of stimulation spots triggering PSCs (x axis) in individual (top, y axis) or across all (bottom) cells grouped by EPSC-only (orange), IPSC-only (blue), or both (purple).

(E) Optically evoked average biphasic, compound PSCs recorded at V_h = −35 mV, in the same neuron as in (C). PSCs are the average of five trials. Inset shows the expanded PSC inside the gray shaded box.

(F) Fitted IPSC/EPSC amplitude relationships for data from six LHb cells (left) and corresponding R^2 values (right). Colors indicate cell identity as in (D).

3 animals; 16–68/96 spots per cell) elicited PSCs. Over 80% of spots that evoked EPSCs also evoked IPSCs, with shared onset timing (204/252; Figures 3C, 3D, and S6A). The amplitudes of EPSCs and IPSCs were typically correlated in each cell, but the IPSC/EPSC ratio varied from cell to cell (Figures 3F and S3E–S3G). These results are consistent with both transmitters being co-released from *Sst*+ axons and detected by the same postsynaptic cell.

In recordings at intermediate potentials (V_h = −27 or −35 mV), we observed biphasic PSCs following photo-stimulation of the same spots at which isolated EPSCs and IPSCs were detected at each reversal potential (Figures 3C and 3E). i_{max} and $-i_{min}$ of

Please cite this article in press as: Kim et al., Co-packaging of opposing neurotransmitters in individual synaptic vesicles in the central nervous system, Neuron (2022), https://doi.org/10.1016/j.neuron.2022.01.007

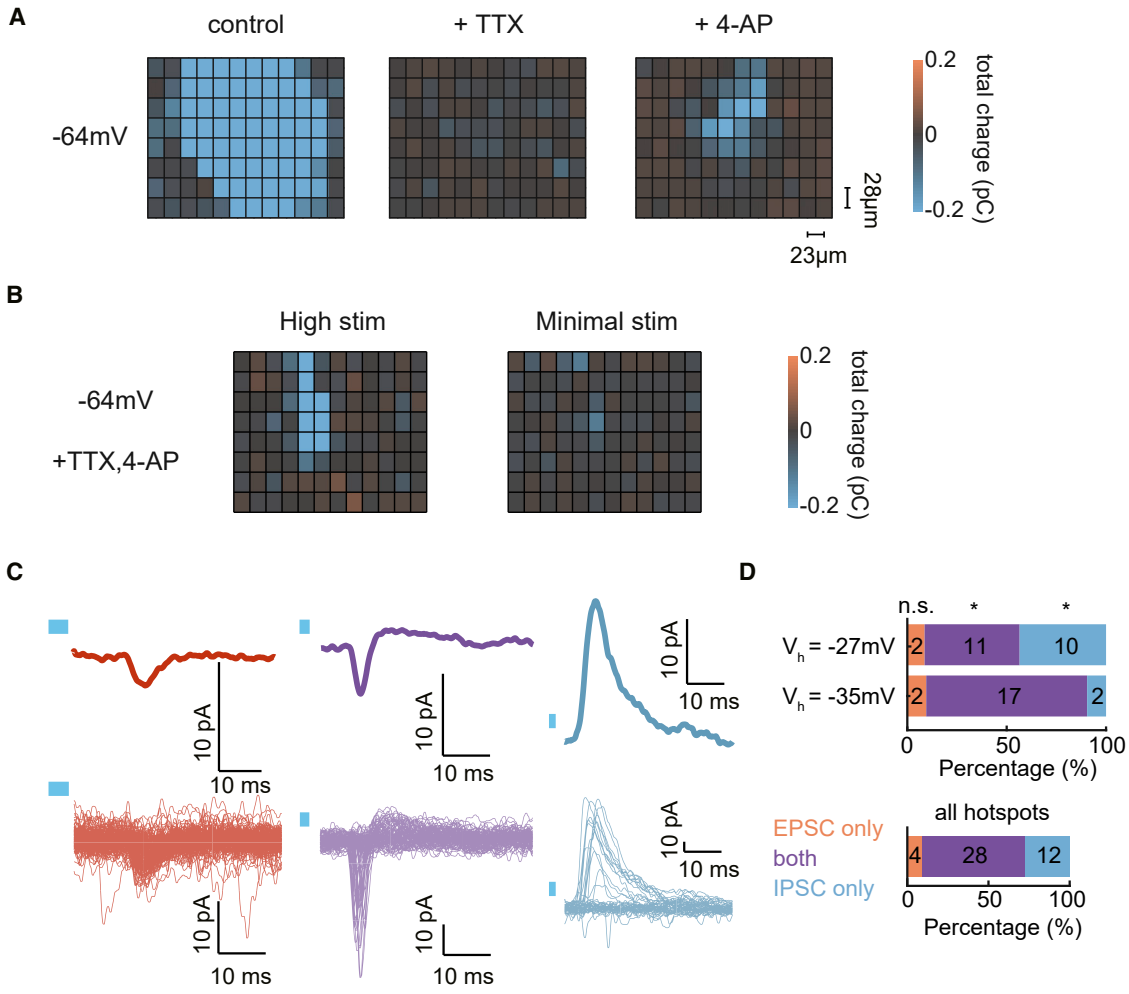

Figure 4. DMOS-evoked unitary responses from EP *Sst*+ axons in LHb

(A) Spatial heatmaps showing the effects of sequential addition of TTX and 4-AP on total charge of EPSCs (V_h = −64mV) of all stimulation spots using DMOS under high photo-stimulation intensity. The cell was located approximately at the center.

(B) Spatial heatmaps comparing total charge of EPSCs (V_h = −64mV) using DMOS under high (top) and minimal (bottom) photo-stimulation intensity.

(C) Average (top) and individual (bottom) unitary PSCs recorded at an intermediate V_h. Repetitive stimulation at three spots consistently evoked EPSC-only (red), IPSC-only (blue), or biphasic (purple) PSCs.

(D) The proportions of minimal stimulation spots that triggered PSCs at V_h = −27 or −35 mV, as indicated (top), or across all cells (bottom) grouped as EPSC-only (orange), IPSC-only (blue), or biphasic (purple). Asterisks indicate statistical significance (Fisher's exact test) of differences in proportions of each group at −27 and −35 mV.

the biphasic PSCs were highly correlated, consistent with these results representing the summation of two oppositely signed synaptic currents (Figure S3I).

Heterogeneity in unitary responses from EP *Sst*+ co-releasing axons

We modified the conditions of DMD-based optogenetic activation to generate minimal responses and called this approach DMOS—DMD-based minimal optogenetic stimulation. Voltage-clamp recordings were performed in the presence of TTX/4-AP to optogenetically activate presynaptic boutons without propagating action potentials (Figure 4A) and prevent polysynaptic responses (Petreanu et al., 2009). We adjusted stimulation intensities and spot sizes to achieve EPSCs that appeared stochastically from trial to trial and whose amplitudes (V_h = −64 mV) were similar to those of miniature spontaneous EPSCs (mEPSCs) (Figure 4B). At −35 or −27 mV, minimally stimulating EP *Sst*+ axons occasionally evoked biphasic PSCs with i_{min} and i_{max} of similar amplitudes to mEPSCs and mIPSCs, respectively (Figures S4E and S4F).

Using DMOS, we observed stimulation spots that evoked "EPSC-only," "IPSC-only," or both currents on every success trial (total trials: 50–205, mean: 111) (Figure 4C). Overall, the majority (~64%) of all hotspots (n = 44, 14 cells) exhibited both PSCs, consistent with the co-packaging model (Figures 4D, S4B–S4D, and S6B–S6E). We hypothesized that some of the "EPSC-only" and "IPSC-only" unitary PSCs resulted from masking of the other current rather than a true lack of IPSC

Please cite this article in press as: Kim et al., Co-packaging of opposing neurotransmitters in individual synaptic vesicles in the central nervous system, Neuron (2022), https://doi.org/10.1016/j.neuron.2022.01.007

and EPSC, due to the reduction of ion channel driving forces at an intermediate V_h. Indeed, the relative proportion of "IPSC-only" hotspots increased to 34% (2/21 → 10/23 hotspots, 7 cells/group, Fisher's test p = 0.0174) when the V_h was increased from −35 to −27 mV (Figure 4D).

Examples of unitary responses that support independent and co-packaging models

Among DMOS-activated spots that generated biphasic PSCs, we found examples consistent with independent (Figures 5A–5E) as well as co-packaging (Figures 5F–5J) models. Note that the common failure modes of our analyses will artificially support a model of independent release of glutamate and GABA.

At sites consistent with independent release, heterogeneous PSCs were observed across trials with i_{min} typically preceding i_{max} (Figure 5A). A scatterplot of $-i_{min}$ versus i_{max} (Figure 5B) revealed a dispersed pattern with a negative slope consistent with the independent model (Figure 2C). Furthermore, a bootstrapped probability distribution of detecting both PSCs in single trials was not different from that expected by chance (Figure 5C). We simulated the biophysical models of the two different co-release modes using the experimental PSC parameters (i.e., the number of trials, p(E), and p(I)). The distributions of the joint probability of detecting i_{max} and i_{min} together matched that generated by the independent model rather than the co-packaging model (Figure 5C). Similarly, cdfs of $-i_{min}$ in trials with or without an IPSC showed no difference (Figure 5D), consistent with the independent model prediction (Figure 2E). The same was true for the i_{max} cdfs. Finally, bootstrapped correlation distributions of i_{max} and $-i_{min}$ pairs were centered around zero for all trials and slightly negative for success trials (Figure 5E). Thus, this set of PSCs generated by DMOS-stimulation of one site 145 times is best described by the independent release model. This conclusion may reflect true independent release and detection of glutamate and GABA at a single synapse or may result from the presence of both a glutamate-only and a GABA-only synapse at the illuminated site.

At sites whose stimulation produced PSCs consistent with co-packaging, all successful event traces consisted of biphasic PSCs (Figure 5F). The scatterplots of i_{max} versus $-i_{min}$ exhibited a positive correlation (Figures 5G and 2C). The bootstrapped probability distribution of detecting both PSCs was significantly greater ($p < 0.001$) than the distribution predicted by chance (Figure 5H). The difference between the distributions disappeared when the i_{max} and $-i_{min}$ were separately shuffled across trials. Furthermore, in agreement with the increased probability of detecting both PSCs in single trials, these data were best fit by simulations of the co-packaging model. In addition, cdfs of the $-i_{min}$ and i_{max} were well separated when comparing across trials categorized by the absence versus presence of an IPSC or EPSC, respectively (Figures 5I and 2E). Lastly, bootstrapped i_{max} and $-i_{min}$ pairs exhibited a large positive correlation for all trials and slightly smaller positive correlation for success trials (Figures 5J and 2F). Hence, our dataset contains PSCs consistent with co-packaging of glutamate and GABA in the same vesicle, a conclusion that is difficult to produce by random events or technical artifacts (Figure S5).

Unitary responses of co-transmitting boutons are consistent with the co-packaging model

For each spot (n = 28, 11 cells) that exhibited DMOS-evoked biphasic PSCs, we performed the full analyses depicted in Figures 5A–5E. To quantify how much each statistical feature supported either model, a "model feature indicator" was parametrized (Figure 6A). This resulted in five model feature indicators that summarize the deviation from random (see STAR Methods).

Extreme values of parameters indicate strong fit by either the co-packaging or independent model, whereas values closer to zero reflect uncertain categorization (Figure 6B). As our study was designed to test whether any synaptic responses were statistically compatible with co-packaging of glutamate/GABA, the model feature indicators were transformed to range from 0 (ambiguous or consistent with independent model) to 1 (high confidence for co-packaging). The heatmap of transformed model feature indicators revealed a column-like structure, indicating consistency in their degree of site-by-site support for the co-packaging model (Figure 6C–6D). Using this metric, 22/28 sites had a feature average greater than 0 (0.0057–0.722, mean = 0.253) (Figure 6E).

To investigate how various failure modes of analyses contribute to our results, we considered three noise metrics (Figure 6F). Two major differences between an ambiguous and a strongly supported co-packaging site were (1) the signal separation between spontaneous activity erroneously picked up by our analysis versus evoked i_{max} and i_{min} and (2) the signal to noise (SNR) of i_{max} and $-i_{min}$ (Figure 6G). At a population level, the sites with the best recording quality (low noise and low spontaneous synaptic events) had greater support for the co-packaging release model (Figures 6H and S5C). This suggests that confounds of recording conditions may underlie the existence of the sites that support the independent model or are ambiguous, such that most, if not all, co-transmitting sites might reflect synapses at which glutamate and GABA are co-packaged.

Pharmacological perturbations confirm co-packaging of glutamate and GABA in individual vesicles

A strong test of the co-packaging model is to examine whether the correlations between glutamatergic and GABAergic PSCs remain when p_r is lowered: if both transmitters are in the same vesicle, then the co-occurrence of evoked inward and outward PSCs should persist, whereas, if release of each transmitter is independent, then an n-fold reduction in p_r should reduce the probability of biphasic PSCs n^2-fold.

5-HT reduces the probability of glutamate and GABA release from the EP axons in the LHb (Shabel et al., 2014, 2012), but it is unknown whether 5-HT has a similar effect on EP *Sst*+ axons or equally on glutamatergic and GABAergic transmission. We examined the effect of 5-HT on PSCs in LHb neurons resulting from activating groups of EP *Sst*+ synapses (Figure 7A). Optogenetic ring stimulation using the DMD elicited composite PSCs in all cells (EPSC median (IQR) = 395 pA (367 pA); IPSC median (IQR) = 624 pA (456 pA); n = 15 cells, 9 animals; Figure 7B), which were blocked by TTX (1 μM) and not recovered by 4-AP (400 μM), consistent with being evoked by propagating action potentials. Application of 5-HT (1 μM) reduced inward and outward

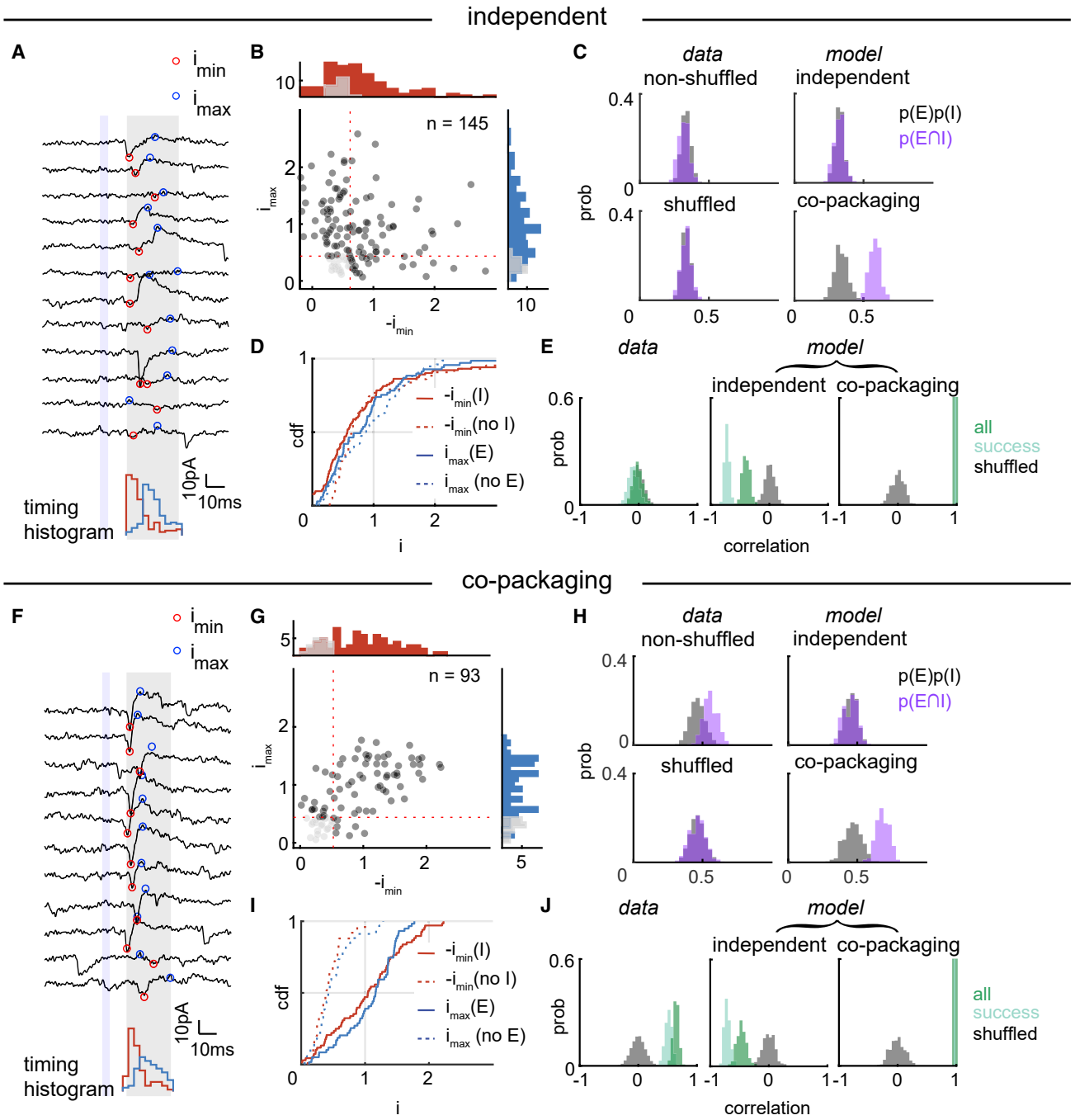

Figure 5. Unitary responses from glutamate/GABA co-releasing boutons

(A) Optically evoked PSCs from a hotspot consistent with the independent model. Top, example traces aligned to stimulus onset (blue region). i_{max} (blue dot) and i_{min} (red dot) were extracted from within the gray region. Bottom, histogram of i_{max} (blue) and i_{min} (red) timing.

(B) Scatterplot of $-i_{min}$ versus i_{max} for all trials at the spot shown in (A).

(C) Comparison of the p(E∩I) (purple) to p(E)*p(I) (gray). Left, histograms of probabilities generated from bootstrap analysis of actual (top) and shuffled (bottom) data. Right, simulated histograms of probabilities generated by independent (top) and co-packaging (bottom) models using synaptic parameters extracted from the data in (B).

(D) Cdfs of i_{max}(E) (blue solid), i_{max}(no E) (blue dashed), $-i_{min}$(I), (red solid), and $-i_{min}$(no I) (red dashed) for data in (B).

(E) Correlation of i_{max} and $-i_{min}$ across all trials (dark green), success trials (light green), and across all trials after shuffling (gray). Bootstrapped correlation coefficients for data from (B) (left) and for results of simulations (parameters as in C) of independent (middle) and co-packaging (right) models.

(F–J) As in (A–E) but for a spot with properties consistent with the co-packaging model.

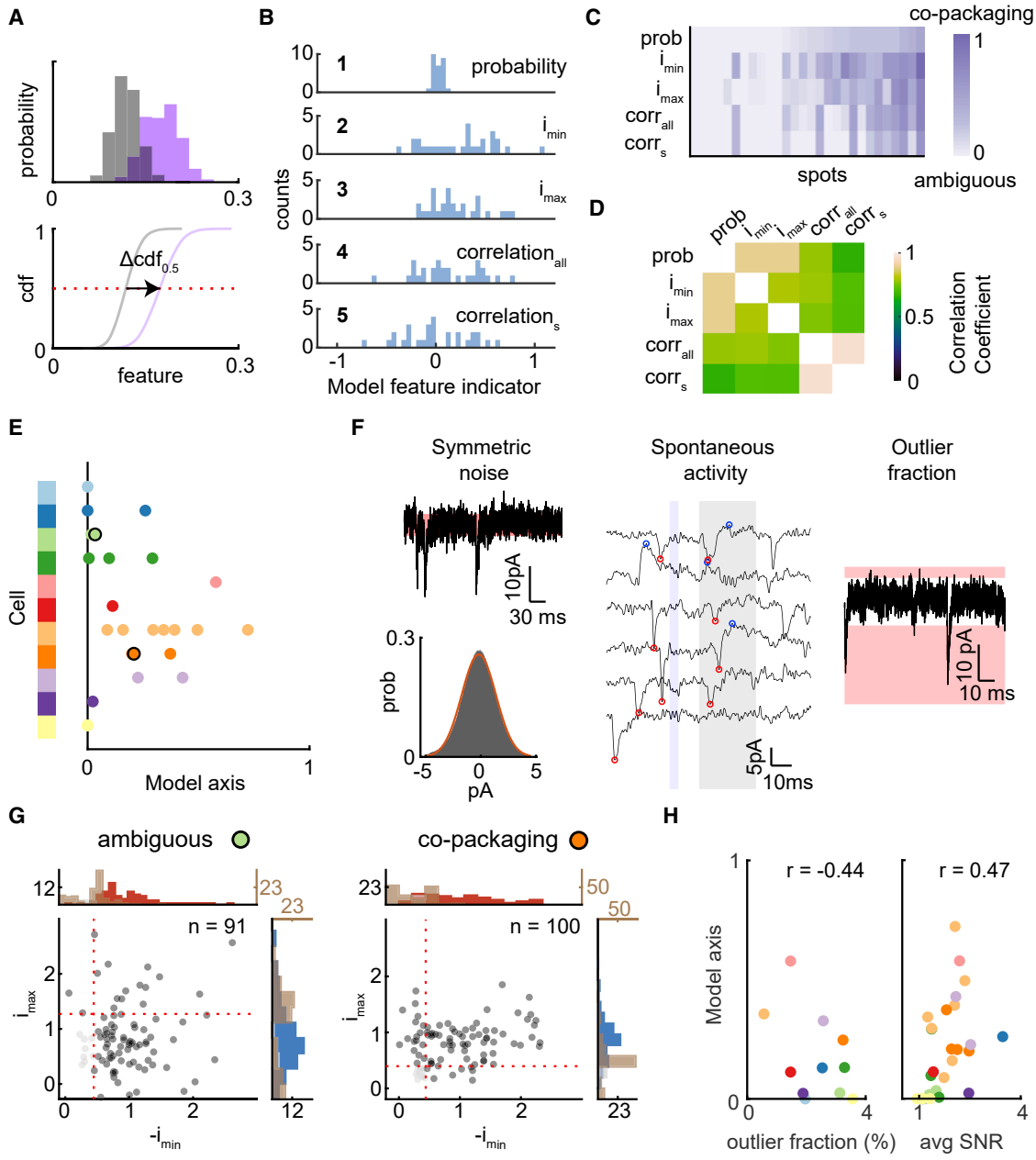

Figure 6. Statistical analyses of all co-releasing terminals support the co-packaging model

(A) Parametrization of a model feature indicator calculated by subtracting the medians of the cdfs ($\Delta cdf_{0.5}$) representing the distributions of p(E∩I) (purple) and p(E)*p(I) (gray).

(B) Histograms of the model feature indicators for the five statistical features. The data represent "both" group in Figure 4F. Bin width is 0.05.

(C) Heatmap of transformed model feature indicators from (B) (y axis) across spots exhibiting both PSCs (x axis). Color intensity represents increasing support for the co-packaging model.

(D) Correlation heatmap of model feature indicators.

(E) Average model feature indicators of all unitary co-releasing spots from (C). Each dot is data from one spot, with color indicating the cell identity. Larger values indicate greater support for the co-packaging model. Data from the black outlined spots are shown in detail in (G).

(F) Three noise sources in the recordings.

(G) Scatterplots of i_{max} and $-i_{min}$ for ambiguous (left, green dot from E) and co-packaging (right, orange dot from E) hotspots. Histograms of the i_{max} and $-i_{min}$ of evoked (right, blue; top, red) and spontaneous (brown) PSCs.

(H) Average model feature indicators for individual spots are correlated with the fraction of outlier current values during baseline periods (left) and the average i_{max} and $-i_{min}$ SNR (right). Colors indicate cells identities as in (E). Pearson correlation coefficients are given.

Please cite this article in press as: Kim et al., Co-packaging of opposing neurotransmitters in individual synaptic vesicles in the central nervous system, Neuron (2022), https://doi.org/10.1016/j.neuron.2022.01.007

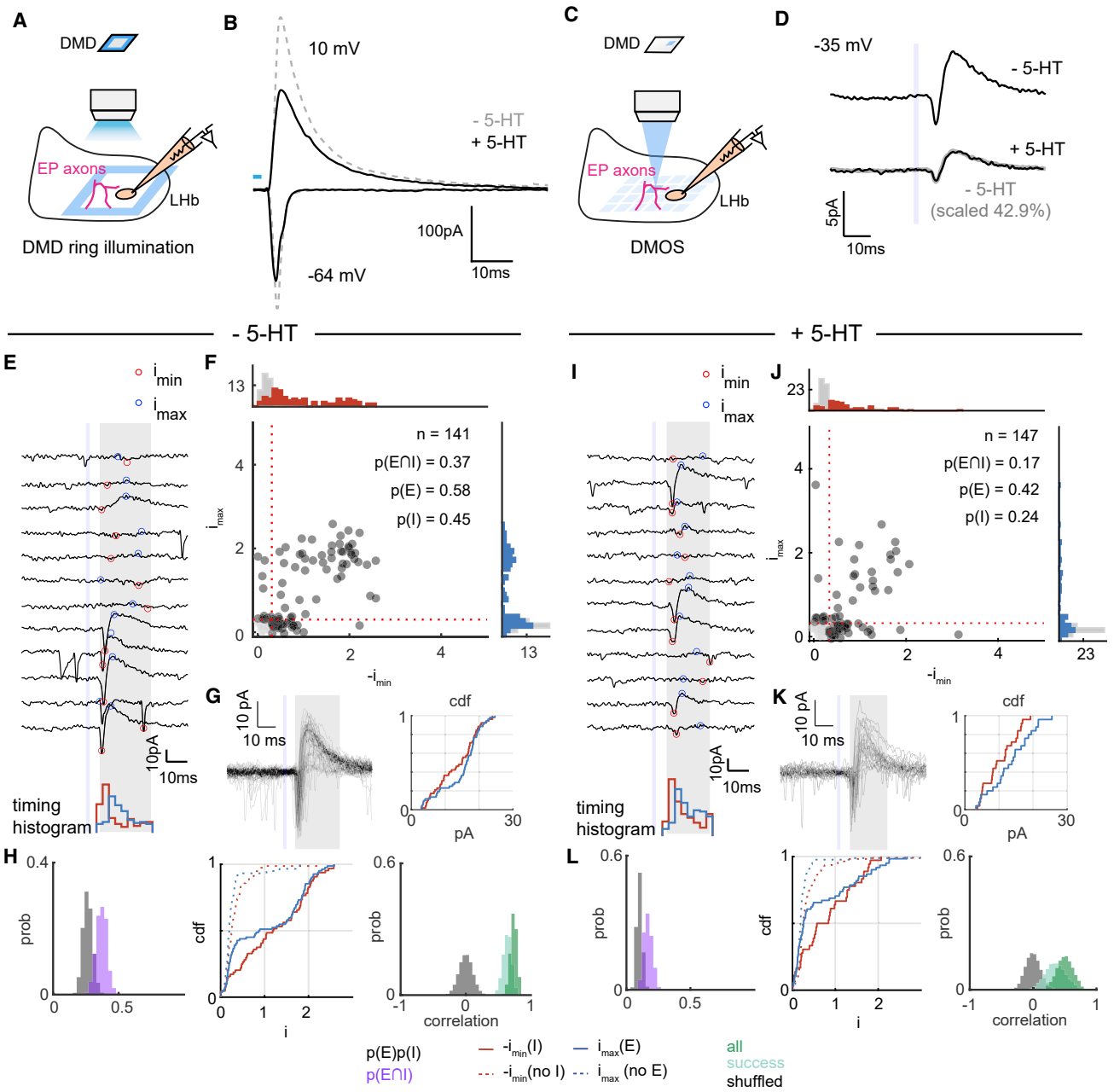

Figure 7. 5-HT reduces p_r of glutamate and GABA while maintaining their co-packaging

(A) DMD ring stimulation used to generate propagating action potentials in EP *Sst*+ axons.

(B) Average EPSC (V_h = −64 mV) and IPSC (V_h = 10 mV) using ring stimulation (blue box) recorded in a LHb neuron before (gray dashed) and after (black) application of 5-HT (1 μM).

(C and D) Schematic of DMOS to activate individual presynaptic boutons (C) and average biphasic PSCs (V_h = −35 mV, black line) before (top, n = 141 trials) and after (bottom, n = 147 trials) application of 5-HT (250 nM) (D). 5-HT proportionally reduced the PSC—the average PSC before 5-HT application is shown scaled and overlaid (gray) on the bottom.

(E) Optically evoked PSCs from a hotspot consistent with the co-packaging model depicted as in Figure 5F.

(F) Scatterplot of i_{max} and $-i_{min}$ for the spot shown in (E), as depicted in Figure 5G. The probabilities of detecting an EPSC, IPSC, and both are given.

(G) Left, optically evoked biphasic unitary PSCs (V_h = −35 mV) of "both" success trials. Right, cdfs of i_{max} (blue) and $-i_{min}$ (red) of these trials.

(H) Analysis of statistical features for the data in (F): left, comparison of the p(E∩I) (purple) to p(E)*p(I) (gray). Middle, cdfs i_{max} (blue) given the presence (solid) or absence (dashed) of an EPSC and vice versa. Right, correlation of i_{max} and $-i_{min}$ across all (dark green), success (light green), and shuffled (gray) trials.

(I–L) As in (E–H) after 5-HT (250 nM) bath application for the same site.

Please cite this article in press as: Kim et al., Co-packaging of opposing neurotransmitters in individual synaptic vesicles in the central nervous system, Neuron (2022), https://doi.org/10.1016/j.neuron.2022.01.007

CellPress

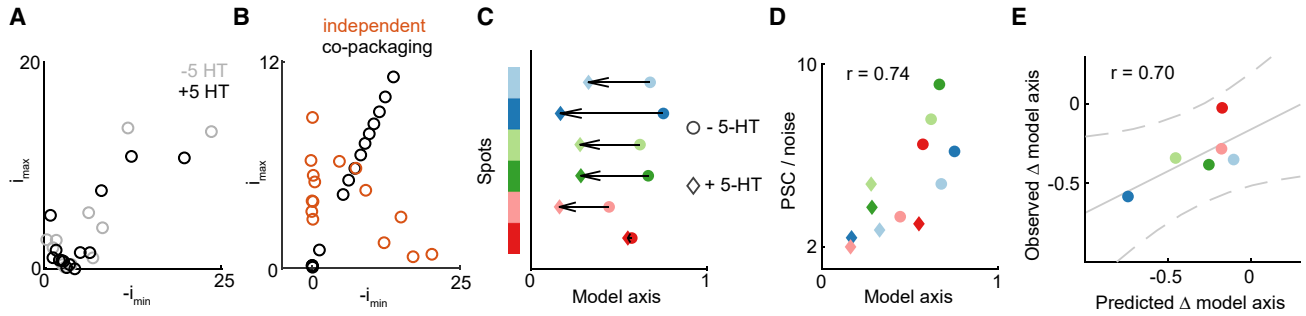

Figure 8. Summary of 5-HT effects on glutamate/GABA co-packaging

(A) 5-HT effect on quantiles of i_{max} and $-i_{min}$ for the data shown in Figures 7E–7L. Dots show the amplitudes of the average trace for quantile of the data before (gray) and after (black) 5-HT application.

(B) As in (A) for showing the predictions of the independent (orange) and co-packaging (black) models.

(C) 5-HT effects on average model feature indicators of unitary co-releasing spots consistent with co-packaging model, based on the statistical features shown in Figure 6C. Arrows indicate the direction of the change due to 5-HT application.

(D) Average ratio between PSC and noise of individual spots versus average model feature indicators. Pearson correlation coefficient is given.

(E) Comparison of observed model axis change due to 5-HT and that predicted by simulation with considering changes in p_r, noise, and amplitudes of biphasic PSCs. Linear fit (solid gray), the 95% prediction interval (dashed), and the Pearson correlation coefficient are shown.

PSCs in most cells (5/6 for EPSC; 6/6 for IPSC; unpaired t test $p < 0.05$; Figure S7A), consistent with inhibition of both glutamate and GABA release from EP *Sst*+ axons. Furthermore, 5HT1b receptor agonist CP93129 (1 μM) reduced inward and outward PSCs (4/4 cells; unpaired t test $p < 0.05$; Figure S7A). In addition, adenosine receptor agonist, 2-chloroadenosine (2-CA), decreased EPSCs and IPSCs in 3/5 and 4/5 cells, respectively (unpaired t test, $p < 0.05$; Figure S7A). Consistent with a reduction in p_r, paired-pulse ratios increased after application of 5-HT (n = 6 cells) and 2-CA (n = 5 cells) (paired t test $p < 0.05$; Figure S7B).

To test whether 5-HT and adenosine receptors modulate biphasic PSCs resulting from activation of individual EP *Sst*+ boutons, we examined the effects of 5-HT and 2-CA on DMOS-evoked hotspots with characteristics consistent with the co-packaging model. A low concentration of 5-HT (0.25 μM) reduced both i_{max} and i_{min} of biphasic PSCs (Figures 7D, 7E, and S7C). Moreover, distributions of i_{max} and i_{min} and the three statistical features were consistent with release under the co-packaging model (Figures 7F and 7H). 5-HT reduced probability of success trials overall as well as of EPSCs, IPSCs, and biphasic PSCs (Figures 7J, 7L, and S7D). Thus, 5-HT reduces both glutamate and GABA release from individual terminals that appear to package both transmitters into individual vesicles.

The distributions of i_{max} and $-i_{min}$ spanned similar ranges before and after 5-HT application (Figures 7F and 7J). Waveforms and the cdfs of the i_{max} and i_{min} of the biphasic PSC trials were comparable (Figures 7G and 7K), and the bootstrapped Kolmogorov-Smirnov (K-S) tests indicated no significant difference between the two groups ($p = 0.4695$ [i_{min}], $p = 0.6924$ [i_{max}]; Table S1). In the same dataset, cdfs of i_{min} and i_{max} of success trials were not significantly different (Table S1). Only 2/6 cells had significantly different cdfs of i_{min}, and only 1/6 had a significantly different i_{max} cdf (Table S1) in "both" success trials. Thus, the major effect of 5-HT on DMOS-evoked unitary PSCs is to reduce probability of release, but it may have additional effects on postsynaptic receptor opening (i.e., synaptic potency). Lastly, we developed an alternative test comparing quantiles of i_{max} and i_{min} distributions before and after drug application, which confirmed that the data were most consistent with a reduction of p_r in the co-packaging model (Figures 8A, 8B, S7E, and S7F).

After 5-HT bath application, the three statistical features of all sites continued to support the co-packaging model (Figures 7H, 7L, and 8C; n = 6/6 spots) such that the mean model indicator value remained >0. Nevertheless, the mean model indicator decreased by 0.33 ± 0.07 (Table S1), as expected from reduced SNR due to (1) effects on synaptic potency or (2) increased current noise and rundown of PSCs that invariably occur during long recordings. Indeed, model indicator values pooled from two conditions were strongly correlated with the ratio of the PSC amplitude and current noise of the individual spots ($r = 0.74$, $p = 0.0063$; Figure 8D). Changes in the p_r, baseline noise, and PSC amplitude in "both" success trials accounted for the observed changes in model indicator value ($r = 0.70$, $p = 0.12$; norm of residuals of fit = 0.29; Figure 8E). These results demonstrate that 5-HT reduces p_r of both glutamate and GABA from EP *Sst*+ inputs to the LHb but that terminals with features consistent with co-packaging continue to exhibit these features after reductions in p_r.

Trial-by-trial analysis of unitary PSCs with DMOS revealed that, after 2-CA (100 μM) application, the statistical features of individual synapses consistent with the co-packaging model are preserved (Figures S8A–S8H). Overall, 2-CA decreased i_{max} and i_{min} of DMOS-evoked biphasic hotspots (Figure S8I; mean number of trials: 103 ± 2.42; n = 4 spots, 4 cells, 4 animals). The observed model indicator value changes induced by 2-CA are well fit by changes in the p_r, baseline noise, and PSC amplitudes (Figures S8K–S8M). In summary, although 5-HT and adenosine receptor agonists reduce glutamate and GABA release from EP *Sst*+ terminals, the statistical features of PSCs in the

Please cite this article in press as: Kim et al., Co-packaging of opposing neurotransmitters in individual synaptic vesicles in the central nervous system, Neuron (2022), https://doi.org/10.1016/j.neuron.2022.01.007

presence of each neuromodulator continue to support the co-packaging model.

DISCUSSION

Here, we describe an experimental and statistical approach that distinguishes between distinct mechanisms of neurotransmitter co-transmission. We identify three statistical features that differentiate between release models in which neurotransmitters are released independently or in which they are packaged in the same synaptic vesicles. We apply this method to analyze glutamate/GABA co-transmission at EP *Sst*+ terminals in LHb and uncover examples of synapses that, when repetitively activated by DMOS, generate PSCs whose properties are consistent only with packaging of both transmitters in the same vesicles. Pharmacological perturbations confirm that the statistical properties expected from release of co-packaged glutamate and GABA are preserved when p_r is lowered. Lastly, the analysis of the effects of recording quality suggests that synapses labeled as more consistent with the independent release of glutamate and GABA may actually reflect co-packaged release, but with the expected correlations between glutamate/GABA currents obscured by noise. Thus, we conclude that EP *Sst*+ neurons package glutamate and GABA into the same vesicles and release them to activate correlated EPSCs and IPSCs in LHb neurons.

EP *Sst*+ axons form glutamate/GABA co-releasing synapses in LHb

We found enrichment of glutamate and GABA vesicular transporters, Vglut2 and Vgat, respectively, in EP *Sst*+ boutons in LHb. High covariance of expression of these presynaptic proteins agrees with ultrastructural analysis supporting that glutamate and GABA are released from the same terminals (Root et al., 2018; Shabel et al., 2014). Curiously, the postsynaptic scaffolding protein gephyrin, but not PSD95, is highly enriched near EP *Sst*+ terminals despite the clear glutamatergic nature of these boutons (Li et al., 2011; Maroteaux and Mameli, 2012). This may indicate that an alternative MAGUK forms the core of these postsynaptic terminals. A positive correlation between Vglut2 expression and that of synapsin-1 and PSD95, across all terminals in LHb, indicates the existence of other molecularly distinct glutamatergic synapses in LHb (Barker et al., 2017; Hu et al., 2020; Knowland et al., 2017; Stamatakis et al., 2016).

The existence of vesicles containing both glutamate and GABA was suggested by the observation of biphasic mPSCs in LHb neurons (Shabel et al., 2014). The source of these responses was unknown since LHb receives projections that release glutamate and GABA from several brain regions (Barker et al., 2017; Stamatakis et al., 2016), including the ventral-tegmental areas (VTAs) (Root et al., 2014a, 2018). Interestingly, although the VTA also sends glutamate/GABA co-releasing axons to LHb, these are thought to release each transmitter from a separate pool of vesicles (Root et al., 2018).

Glutamate/GABA co-packaging may result from expression of Vglut2 and Vgat on the same vesicle. The number of transporter proteins on each vesicle is ~10 (Takamori et al., 2006), suggesting that individual vesicles may accommodate more than one type of transporter. As the number of vesicular transporters determines the amount of neurotransmitter loaded into vesicles (Wojcik et al., 2004), the number of Vglut2 and Vgat per vesicle may determine the glutamate/GABA content and its variability across vesicles.

Function of the EP, LHb, and co-release

EP neurons preferentially target LHb neurons projecting to GABAergic rostromedial tegmental nucleus neurons (Meye et al., 2016), suggesting an indirect function of EP *Sst*+ neurons in regulating dopamine release. Since increased LHb activity can have aversive and reinforcing effects (Lammel et al., 2012; Proulx et al., 2014; Stamatakis and Stuber, 2012), the net ratio of glutamate/GABA released from EP *Sst*+ terminals may determine the behavioral consequence resulting from modulation of these cells. Indeed, GABA transmission from EP to LHb is altered by experience, resulting in changes in the ratio of glutamate/GABA currents (Lalive et al., 2021; Meye et al., 2016).

The ratios of glutamate/GABA currents from multiple synapses are similar in each postsynaptic LHb neuron but differ across LHb neurons. We speculate that co-packaging glutamate and GABA into the same vesicles grants flexibility to LHb neurons in determining the transformation calculated from a common set of EP *Sst*+ inputs via changes in postsynaptic receptor composition. This allows each LHb neuron to have net inhibitory or excitatory effects from activity in the same EP *Sst*+ inputs and to choose the synaptic sign and weight that best predict an aversive outcome. Thus, negative weights are assigned to inputs whose activity coincides with or predicts a good outcome, and positive weights are assigned to those associated with bad outcomes.

Compared with the net effect and function of glutamate/GABA co-release from EP terminals to LHb neurons, the function of co-release from VTA terminals in LHb has been better characterized. Activating VTA-to-LHb glutamate/GABA co-releasing neurons inhibits most and excites some postsynaptic LHb neurons (Root et al., 2014b). Moreover, VTA-to-LHb glutamate/GABA co-releasing neurons signal rewarding or aversive outcomes without responding to learned predictors in classical conditioning tasks (Root et al., 2020). Thus, these glutamate/GABA co-releasing neurons, such as VTA dopamine neurons, encode violations of reward expectations.

Neuromodulation of glutamate and GABA co-releasing neurons

Applications of 5-HT or adenosine receptor agonists reduce the amplitude of EPSCs and IPSCs evoked in LHb neurons by stimulation of EP *Sst*+ axons. This is consistent with previous conclusions that 5-HT reduces the probabilities of glutamate and GABA release from EP axons (Shabel et al., 2012, 2014). We show that this effect is due, in part at least, to effects on *Sst*+ EP inputs and additionally demonstrate that these synapses are also modulated by adenosine receptors. In synapses that co-package glutamate/GABA, the major effect of 5-HT as well as of 2-CA is to decrease the p_r of these vesicles with a potential additional effect on synaptic potency. 5-HT 1B and adenosine A1 receptors are both predicted to be expressed in EP *Sst*+ neurons and likely mediate the presynaptic effect of 5-HT and 2-CA, respectively, through $G_{i/o}$-mediated

signaling (Figure S7A) (Hwang and Chung, 2014; Wallace et al., 2017).

5-HT signaling in LHb has been investigated in the context of depression and its treatment. In animal models of depression, presynaptic changes have been described that shift the ratio of EP-to-LHb glutamate/GABA transmission, and this effect is reversed by treatment with selective serotonin reuptake inhibitor (SSRI)-type antidepressants (Shabel et al., 2014). Although our results suggest that the short-term effect of 5-HT is to inhibit release from *Sst*+ inputs in LHb, long-term additional effects of 5-HT on glutamate/GABA co-packaging vesicles remain unknown.

STAR★METHODS

Detailed methods are provided in the online version of this paper and include the following:

- KEY RESOURCES TABLE
- RESOURCE AVAILABILITY
  - Lead contact
  - Materials availability
  - Data and code availability
- EXPERIMENTAL MODEL AND SUBJECT DETAILS
  - Mice
- METHOD DETAILS
  - Viruses
  - Intracranial virus injections
  - Array tomography
  - DMOS optical setup
  - Acute brain slice preparation
  - Electrophysiology
  - Model simulations
  - Analysis of electrophysiology data
  - DMOS spatial heatmaps
  - 3 Statistical features
  - Parametrization of model feature indicator
  - Three types of noise metrics
  - Analysis of 5-HT pharmacological effect
  - Technical concerns involving our study of glutamate/GABA co-release
- QUANTIFICATION AND STATISTICAL ANALYSIS

SUPPLEMENTAL INFORMATION

Supplemental information can be found online at https://doi.org/10.1016/j.neuron.2022.01.007.

ACKNOWLEDGMENTS

We thank A. Bègue, P. Gorelik, and O. Mazor for technical help; M. El-Rifai and A. Granger for help with array tomography; and Sabatini lab members for helpful discussions. This work was supported by NIH (R01NS103226 to B.L.S., R00NS105883-03 to M.L.W., and P30NS072030 to the Neurobiology Imaging Facility).

AUTHOR CONTRIBUTIONS

S.K., M.L.W., and B.L.S. designed experiments and analyses. S.K. and B.L.S. built the DMOS system and developed computational models and analysis methods. S.K. performed all experiments and analyses except those in Figure 1. M.L.W. and M.E.-R. collected array tomography data. A.R.K. performed intracranial injections and histology. S.K. and B.L.S. wrote the manuscript with feedback from all authors.

DECLARATION OF INTERESTS

B.L.S. is a member of the *Neuron* advisory board.

Received: March 25, 2021
Revised: November 16, 2021
Accepted: January 6, 2022
Published: February 3, 2022

REFERENCES

Barker, D.J., Miranda-Barrientos, J., Zhang, S., Root, D.H., Wang, H.-L., Liu, B., Calipari, E.S., and Morales, M. (2017). Lateral preoptic control of the lateral habenula through convergent glutamate and GABA transmission. Cell Rep *21*, 1757–1769. https://doi.org/10.1016/j.celrep.2017.10.066.

Cerniauskas, I., Winterer, J., de Jong, J.W., Lukacsovich, D., Yang, H., Khan, F., Peck, J.R., Obayashi, S.K., Lilascharoen, V., Lim, B.K., et al. (2019). Chronic stress induces activity, synaptic, and transcriptional remodeling of the lateral habenula associated with deficits in motivated behaviors. Neuron *104*. 899.e8–915.e8. https://doi.org/10.1016/j.neuron.2019.09.005.

Granger, A.J., Wang, W., Robertson, K., El-Rifai, M., Zanello, A.F., Bistrong, K., Saunders, A., Chow, B.W., Nuñez, V., Turrero García, M., et al. (2020). Cortical ChAT+ neurons co-transmit acetylcholine and GABA in a target- and brain-region-specific manner. eLife *9*, e57749. https://doi.org/10.7554/eLife.57749.

Hong, S., and Hikosaka, O. (2008). The globus pallidus sends reward-related signals to the lateral habenula. Neuron *60*, 720–729. https://doi.org/10.1016/j.neuron.2008.09.035.

Hu, H., Cui, Y., and Yang, Y. (2020). Circuits and functions of the lateral habenula in health and in disease. Nat. Rev. Neurosci. *21*, 277–295. https://doi.org/10.1038/s41583-020-0292-4.

Hwang, E.-K., and Chung, J.M. (2014). 5HT(1B) receptor-mediated pre-synaptic depression of excitatory inputs to the rat lateral habenula. Neuropharmacology *81*, 153–165. https://doi.org/10.1016/j.neuropharm.2014.01.046.

Jonas, P., Bischofberger, J., and Sandkühler, J. (1998). Corelease of two fast neurotransmitters at a central synapse. Science *281*, 419–424. https://doi.org/10.1126/science.281.5375.419.

Knowland, D., Lilascharoen, V., Pacia, C.P., Shin, S., Wang, E.H.-J., and Lim, B.K. (2017). Distinct ventral pallidal neural populations mediate separate symptoms of depression. Cell *170*. 284.e18–297.e18. https://doi.org/10.1016/j.cell.2017.06.015.

Lalive, A.L., Congiu, M., Clerke, J.A., Tchenio, A., Ge, Y., and Mameli, M. (2021). Synaptic inhibition in the lateral habenula shapes reward anticipation. bioRxiv. https://doi.org/10.1101/2021.01.21.427572.

Lammel, S., Lim, B.K., Ran, C., Huang, K.W., Betley, M.J., Tye, K.M., Deisseroth, K., and Malenka, R.C. (2012). Input-specific control of reward and aversion in the ventral tegmental area. Nature *491*, 212–217. https://doi.org/10.1038/nature11527.

Lee, S., Kim, K., and Zhou, Z.J. (2010). Role of ACh-GABA cotransmission in detecting image motion and motion direction. Neuron *68*, 1159–1172. https://doi.org/10.1016/j.neuron.2010.11.031.

Li, B., Piriz, J., Mirrione, M., Chung, C., Proulx, C.D., Schulz, D., Henn, F., and Malinow, R. (2011). Synaptic potentiation onto habenula neurons in the learned helplessness model of depression. Nature *470*, 535–539. https://doi.org/10.1038/nature09742.

Li, H., Pullmann, D., and Jhou, T.C. (2019). Valence-encoding in the lateral habenula arises from the entopeduncular region. eLife *8*, e41223. https://doi.org/10.7554/eLife.41223.

Lin, J.Y., Lin, M.Z., Steinbach, P., and Tsien, R.Y. (2009). Characterization of engineered channelrhodopsin variants with improved properties and kinetics. Biophys. J. *96*, 1803–1814. https://doi.org/10.1016/j.bpj.2008.11.034.

Maroteaux, M., and Mameli, M. (2012). Cocaine evokes projection-specific synaptic plasticity of lateral habenula neurons. J. Neurosci. *32*, 12641–12646. https://doi.org/10.1523/JNEUROSCI.2405-12.2012.

Matsumoto, M., and Hikosaka, O. (2007). Lateral habenula as a source of negative reward signals in dopamine neurons. Nature *447*, 1111–1115. https://doi.org/10.1038/nature05860.

Matsumoto, M., and Hikosaka, O. (2009). Two types of dopamine neuron distinctly convey positive and negative motivational signals. Nature *459*, 837–841. https://doi.org/10.1038/nature08028.

Meye, F.J., Soiza-Reilly, M., Smit, T., Diana, M.A., Schwarz, M.K., and Mameli, M. (2016). Shifted pallidal co-release of GABA and glutamate in habenula drives cocaine withdrawal and relapse. Nat. Neurosci. *19*, 1019–1024. https://doi.org/10.1038/nn.4334.

Micheva, K.D., and Smith, S.J. (2007). Array tomography: a new tool for imaging the molecular architecture and ultrastructure of neural circuits. Neuron *55*, 25–36. https://doi.org/10.1016/j.neuron.2007.06.014.

Petreanu, L., Huber, D., Sobczyk, A., and Svoboda, K. (2007). Channelrhodopsin-2-assisted circuit mapping of long-range callosal projections. Nat. Neurosci. *10*, 663–668. https://doi.org/10.1038/nn1891.

Petreanu, L., Mao, T., Sternson, S.M., and Svoboda, K. (2009). The subcellular organization of neocortical excitatory connections. Nature *457*, 1142–1145. https://doi.org/10.1038/nature07709.

Proulx, C.D., Hikosaka, O., and Malinow, R. (2014). Reward processing by the lateral habenula in normal and depressive behaviors. Nat. Neurosci. *17*, 1146–1152. https://doi.org/10.1038/nn.3779.

Root, D.H., Barker, D.J., Estrin, D.J., Miranda-Barrientos, J.A., Liu, B., Zhang, S., Wang, H.L., Vautier, F., Ramakrishnan, C., Kim, Y.S., et al. (2020). Distinct signaling by ventral tegmental area glutamate, GABA, and combinatorial glutamate-GABA neurons in motivated behavior. Cell Rep *32*, 108094. https://doi.org/10.1016/j.celrep.2020.108094.

Root, D.H., Mejias-Aponte, C.A., Qi, J., and Morales, M. (2014a). Role of glutamatergic projections from ventral tegmental area to lateral habenula in aversive conditioning. J. Neurosci. *34*, 13906–13910. https://doi.org/10.1523/JNEUROSCI.2029-14.2014.

Root, D.H., Mejias-Aponte, C.A., Zhang, S., Wang, H.-L., Hoffman, A.F., Lupica, C.R., and Morales, M. (2014b). Single rodent mesohabenular axons release glutamate and GABA. Nat. Neurosci. *17*, 1543–1551. https://doi.org/10.1038/nn.3823.

Root, D.H., Zhang, S., Barker, D.J., Miranda-Barrientos, J., Liu, B., Wang, H.-L., and Morales, M. (2018). Selective brain distribution and distinctive synaptic architecture of dual glutamatergic-GABAergic neurons. Cell Rep *23*, 3465–3479. https://doi.org/10.1016/j.celrep.2018.05.063.

Saunders, A., Granger, A.J., and Sabatini, B.L. (2015). Corelease of acetylcholine and GABA from cholinergic forebrain neurons. eLife *4*. e06412. https://doi.org/10.7554/eLife.06412.

Schindelin, J., Arganda-Carreras, I., Frise, E., Kaynig, V., Longair, M., Pietzsch, T., Preibisch, S., Rueden, C., Saalfeld, S., Schmid, B., et al. (2012). Fiji: an open-source platform for biological-image analysis. Nature Methods *9*, 676–682. https://doi.org/10.1038/nmeth.2019.

Shabel, S.J., Proulx, C.D., Piriz, J., and Malinow, R. (2014). Mood regulation. GABA/glutamate co-release controls habenula output and is modified by antidepressant treatment. Science *345*, 1494–1498. https://doi.org/10.1126/science.1250469.

Shabel, S.J., Proulx, C.D., Trias, A., Murphy, R.T., and Malinow, R. (2012). Input to the lateral habenula from the basal ganglia is excitatory, aversive, and suppressed by serotonin. Neuron *74*, 475–481. https://doi.org/10.1016/j.neuron.2012.02.037.

Stamatakis, A.M., and Stuber, G.D. (2012). Activation of lateral habenula inputs to the ventral midbrain promotes behavioral avoidance. Nat. Neurosci. *15*, 1105–1107. https://doi.org/10.1038/nn.3145.

Stamatakis, A.M., Van Swieten, M., Basiri, M.L., Blair, G.A., Kantak, P., and Stuber, G.D. (2016). Lateral hypothalamic area glutamatergic neurons and their projections to the lateral habenula regulate feeding and reward. J. Neurosci. *36*, 302–311. https://doi.org/10.1523/JNEUROSCI.1202-15.2016.

Stephenson-Jones, M., Yu, K., Ahrens, S., Tucciarone, J.M., van Huijstee, A.N., Mejia, L.A., Penzo, M.A., Tai, L.-H., Wilbrecht, L., and Li, B. (2016). A basal ganglia circuit for evaluating action outcomes. Nature *539*, 289–293. https://doi.org/10.1038/nature19845.

Takamori, S., Holt, M., Stenius, K., Lemke, E.A., Grønborg, M., Riedel, D., Urlaub, H., Schenck, S., Brügger, B., Ringler, P., et al. (2006). Molecular anatomy of a trafficking organelle. Cell *127*, 831–846. https://doi.org/10.1016/j.cell.2006.10.030.

Taniguchi, H., He, M., Wu, P., Kim, S., Paik, R., Sugino, K., Kvitsiani, D., Fu, Y., Lu, J., Lin, Y., et al. (2011). A resource of Cre driver lines for genetic targeting of GABAergic neurons in cerebral cortex. Neuron *71*, 995–1013. https://doi.org/10.1016/j.neuron.2011.07.026.

Tritsch, N.X., Ding, J.B., and Sabatini, B.L. (2012). Dopaminergic neurons inhibit striatal output through non-canonical release of GABA. Nature *490*, 262–266. https://doi.org/10.1038/nature11466.

Tritsch, N.X., Granger, A.J., and Sabatini, B.L. (2016). Mechanisms and functions of GABA co-release. Nat. Rev. Neurosci. *17*, 139–145. https://doi.org/10.1038/nrn.2015.21.

Trusel, M., Nuno-Perez, A., Lecca, S., Harada, H., Lalive, A.L., Congiu, M., Takemoto, K., Takahashi, T., Ferraguti, F., and Mameli, M. (2019). Punishment-predictive cues guide avoidance through potentiation of hypothalamus-to-habenula synapses. Neuron *102*. 120.e4–127.e4. https://doi.org/10.1016/j.neuron.2019.01.025.

Wallace, M.L., Saunders, A., Huang, K.W., Philson, A.C., Goldman, M., Macosko, E.Z., McCarroll, S.A., and Sabatini, B.L. (2017). Genetically distinct parallel pathways in the entopeduncular nucleus for limbic and sensorimotor output of the basal ganglia. Neuron *94*. 138.e5–152.e5. https://doi.org/10.1016/j.neuron.2017.03.017.

Wojcik, S.M., Rhee, J.S., Herzog, E., Sigler, A., Jahn, R., Takamori, S., Brose, N., and Rosenmund, C. (2004). An essential role for vesicular glutamate transporter 1 (VGLUT1) in postnatal development and control of quantal size. Proc. Natl. Acad. Sci. USA *101*, 7158–7163. https://doi.org/10.1073/pnas.0401764101.

Yang, Y., Cui, Y., Sang, K., Dong, Y., Ni, Z., Ma, S., and Hu, H. (2018). Ketamine blocks bursting in the lateral habenula to rapidly relieve depression. Nature *554*, 317–322. https://doi.org/10.1038/nature25509.

Zhang, S., Qi, J., Li, X., Wang, H.-L., Britt, J.P., Hoffman, A.F., Bonci, A., Lupica, C.R., and Morales, M. (2015). Dopaminergic and glutamatergic microdomains in a subset of rodent mesoaccumbens axons. Nat. Neurosci. *18*, 386–392. https://doi.org/10.1038/nn.3945.

Please cite this article in press as: Kim et al., Co-packaging of opposing neurotransmitters in individual synaptic vesicles in the central nervous system, Neuron (2022), https://doi.org/10.1016/j.neuron.2022.01.007

STAR★METHODS

KEY RESOURCES TABLE

REAGENT or RESOURCE	SOURCE	IDENTIFIER
Antibodies		
chicken α-GFP	GeneTex	GeneTex Cat# GTX13970; RRID:AB_371416
mouse α-Gephyrin	Biosciences Pharmigen	BD Biosciences Cat# 612632; RRID:AB_399669
rabbit α-Synapsin-1	Cell Signaling Tech	Cell Signaling Technology Cat# 5297; RRID:AB_2616578
rabbit α-PSD95	Cell Signaling Tech	Cell Signaling Technology Cat# 3450; RRID:AB_2292883
mouse α-VGAT	Synaptic Systems	Synaptic Systems Cat# 131 011; RRID:AB_887872
rabbit α-VGLUT2	Synaptic Systems	Synaptic Systems Cat# 135 403; RRID:AB_887883
Bacterial and Virus Strains		
AAV8-EF1α-DIO-oChIEF(E163A/T199C)-P2A-dTomato-WPRE-BGHpA	Lin et al., 2009, Boston Children's Hospital Viral Core	RRID:Addgene_51094
AAV8-CMV-DIO-Synaptophysin-YFP	UNC Vector Core	N/A
Chemicals, Peptides, and Recombinant Proteins		
Serotonin hydrochloride	Tocris	Cat# 3547
2-Chloroadenosine	Tocris	Cat# 3136
CP93129 hydrochloride	Tocris	Cat# 1032
AM251	Tocris	Cat# 1117
(R)-CPP	Tocris	Cat# 0247
Tetrodotoxin citrate (TTX)	Abcam	Cat# 120055
4-Aminopyridine (4-AP)	Tocris	Cat# 0940
Deposited Data		
Raw data files for electrophysiology recordings	This paper	GitHub: https://github.com/seulah-kim/coreleaseAnalysis_Kim2021 https://doi.org/10.5281/zenodo.5810663
Experimental Models: Organisms/Strains		
Mouse: Sst-Cre: *Sst*$^{tm2.1(cre)Zjh}$/J	Jackson Laboratories	Cat# 013044; MGI# 4838416
Mouse: C57BL/6J	Jackson Laboratories	Cat# 000664; MGI# 3028467
Software and Algorithms		
Fiji	Schindelin et al., 2012	https://imagej.net/software/fiji/
MATLAB	MathWorks	https://www.mathworks.com/
Custom MATLAB scripts	SeulAh Kim	GitHub: https://github.com/seulah-kim/coreleaseAnalysis_Kim2021; https://doi.org/10.5281/zenodo.5810663
ScanImage (2015b version)	Bernardo Sabatini	https://github.com/bernardosabatini/SabalabAcq.git
Other		
Digital Micromirror Device	Texas Instruments	DLP LightCrafter Evaluation Module

RESOURCE AVAILABILITY

Lead contact

Further information and requests for resources and reagents should be directed to and will be fulfilled by the lead contact, Bernardo L. Sabatini (bsabatini@hms.harvard.edu)

Materials availability

This study did not generate new unique reagents.

Data and code availability

- Electrophysiology data have been deposited at Zenodo. Accession numbers are listed in the key resources table. Array tomography data reported in this paper will be shared by the lead contact upon request.

Please cite this article in press as: Kim et al., Co-packaging of opposing neurotransmitters in individual synaptic vesicles in the central nervous system, Neuron (2022), https://doi.org/10.1016/j.neuron.2022.01.007

- All custom code for analyzing this data is publicly available as of the date of publication. DOIs are listed in the key resources table.
- Any additional information required to reanalyze the data reported in this paper is available from the lead contact upon request.

EXPERIMENTAL MODEL AND SUBJECT DETAILS

Mice

Sst-Cre (Jackson Labs #013044; MGI #4838416) homozygous and heterozygous mice (C57BL/6; 129 background) were bred with C57BL/6J mice. Both sexes of mice between the ages of 2 and 6 months were used. All animal care and experimental manipulations were performed in accordance with protocols approved by the Harvard Standing Committee on Animal Care, following guidelines described in the US NIH *Guide for the Care and Use of Laboratory Animals*.

METHOD DETAILS

Viruses

To achieve specific expression of light-gated cation channel in the *Sst*+ population in EP, we used a Cre-dependent adeno-associated virus (AAV) that encodes oChIEF, a variant of channelrhodopsin (Lin et al., 2009), driven by the EF1a promoter (AAV8-EF1a-DIO-oChIEF(E163A/T199C)-P2A-dTomato-WPRE-BGHpA). The plasmid was commercially obtained from Addgene (#51094), and the AAV was packaged by Boston Children's Hospital Viral Core. For intracranial injections, the virus was diluted to a titer of ~9 x 10^{12} gc/ml.

Intracranial virus injections

Adult mice (>P50) were anesthetized with 2%–3% isoflurane. Under the stereotaxic frame (David Kopf Instruments), the skull was exposed in aseptic conditions, and the virus was injected bilaterally into the EP (coordinates: -1.0 mm A/P, +/− 2.1 mm M/L, and 4.2 mm D/V, from bregma) through a pulled glass pipette at a rate of 50 nl/min with a UMP3 microsyringe pump (World Precision Instruments). 150 nl was infused per injection site. At least 4 weeks passed after virus injection before experiments were performed.

Array tomography

Mice injected with AAV(8)-CMV-DIO-Synaptophysin-YFP in EP were deeply anesthetized, perfused transcardially with room temperature phosphate-buffered saline (PBS) followed by 4% paraformaldehyde (PFA) in PBS. The brain was removed from the skull, post-fixed overnight at 4°C in 4% PFA, rinsed, and stored in PBS. 250-μm-thick coronal sections were cut with a Leica VT1000s vibratome. Sections containing the habenula with high Synaptophysin-YFP expression were noted using an epifluorescence microscope, and approximately 0.5 × 0.5 mm squares of tissue were cut out under a dissecting scope with Microfeather disposable ophthalmic scalpels. These small tissue squares were then dehydrated with serial alcohol dilutions and infiltrated with LR White acrylic resin (Sigma Aldrich L9774), and placed in a gel cap filled with LR White to polymerize overnight at 50°C. Blocks of tissue were sliced on an ultramicrotome (Leica EM UC7) into ribbons of 70-nm sections.

Antibody staining of these sections was performed as described previously (Saunders et al., 2015). Briefly, antibodies were applied across multiple staining sessions (up to three antibodies per session) and a fourth channel left for DAPI. Typically, Session 1 stained against YFP (chicken α-GFP, GTX13970, GeneTex), Gephyrin (mouse α-Gephyrin, 612632, Biosciences Pharmingen), and Synapsin-1 (rabbit α-Synapsin-1, 5297S, Cell Signaling Tech); Session 2 for PSD-95 (rabbit α-PSD95, 3450 Cell Signaling Tech.); and Session 3 for Vgat (mouse α-VGAT, 131 011 Synaptic Systems) and VGLUT2 (rabbit α-VGLUT2, 135 403 Synaptic Systems). In one sample the staining order was reversed, which revealed that order-dependent differences in staining quality did not alter the analysis. Each round of staining was imaged on a Zeiss Axio Imager upright fluorescence microscope before the tissue ribbons were stripped of antibody and re-stained for a new imaging session. Four images were acquired with a 63× oil objective (Zeiss) and stitched into a single final image (Mosaix, Axiovision). Image stacks were processed by aligning in Fiji (Schindelin et al., 2012) with the MultiStackReg plug-in, first on the DAPI nuclear stain and with fine alignments performed using the Synapsin 1 stack. Fluorescence intensity was normalized across all channels, such that the top and bottom 0.1% of fluorescence intensities were set to 0 and maximum intensity, respectively.

Image analysis was performed as described previously (Granger et al., 2020). Pre-processing steps included trimming the image edges and masking out regions that correspond to cell nuclei as defined by DAPI signal. Background subtraction was performed at a rolling ball radius of 10 pixels in Fiji with the Rolling Ball Background Subtraction plug-in. Synaptophysin-YFP channel was used to create 3D binary masks corresponding to EP *Sst*+ terminals.

For colocalization analysis, antibody fluorescence puncta were fit with a gaussian distribution to identify and assign a pixel location corresponding to the centroid of the gaussian. The YFP mask was overlaid to the antibody puncta location distributions and colocalization was calculated as the number of pixels that overlapped within the YFP mask divided by the total number of pixels of the YFP mask. To estimate colocalization level by chance, the locations of each centroid were randomized prior to colocalization calculation. This randomization was repeated 1,000 times to used calculate a *Z* score per sample per antibody signal to pool across samples (Figure S1).

Please cite this article in press as: Kim et al., Co-packaging of opposing neurotransmitters in individual synaptic vesicles in the central nervous system, Neuron (2022), https://doi.org/10.1016/j.neuron.2022.01.007

In a cross-correlation analysis that does not require identifying individual immunopuncta, each antibody stack was *Z* scored, and two stacks from the same sample were compared by shifting one image up to ±10 pixels in increments of 1 pixel vertically and horizontally. At each shift, the covariance of the images were calculated (Figure 1F). Covariance was also measured specifically within the YFP mask by restricting the above calculation to the image area within the YFP mask (Figure 1G).

DMOS optical setup

A digital micromirror device (DMD) surface was exposed from a DLP LightCrafter Evaluation Module (Texas Instruments) and mounted in the optical path to direct the reflected laser beam to the back aperture of a 0.8 NA 40× objective lens (Olympus). A 473-nm collimated beam of width ~1mm was emitted from the laser (gem 473, Laser Quantum) and was uncollimated by passing through a static holographic diffuser (Edmund Optics) at a 10° divergence angle. A mechanical shutter (Uniblitz, model LS6Z2) was mounted between the laser and the diffuser to control the timing of light exposure. The uncollimated, divergent light after the diffuser was converged using a lens (f = 30 mm) to cover the DMD surface. The diffracted beam from the DMD was collected by a second lens (f = 100 mm) and relayed to the back aperture of the objective to form a conjugated DMD image in the sample plane. The optical setup achieved 22× magnification of the DMD image onto the sample plane with a resultant field-of-view of 299 μm (width) × 168 μm (height).

Custom software written for ScanImage in MATLAB was used to control the individual DMD mirrors. Light power was controlled using Laser Quantum RemoteApp software via the RS232 port. The power efficiency of the system was ~5% from laser output to specimen, resulting in a maximum power of 10 mW at the sample plane when all mirrors were in the "on" position. The validation of the DMD alignment using electrophysiological recording was performed as shown in Figure S3.

Acute brain slice preparation

Acute brain slices were obtained from adult mice anesthetized by isoflurane inhalation and perfused transcardially with ice-cold, carbogen-saturated artificial cerebral spinal fluid (aCSF) containing (in mM) 125 NaCl, 2.5 KCl, 25 $NaHCO_3$, 1.25 NaH_2PO_4, 2 $CaCl_2$, 1 $MgCl_2$, and 17 glucose (300 mOsm/kg). The brain was dissected, blocked, and transferred into a tissue-slicing chamber containing ice-cold aCSF. 250- to 300-μm-thick coronal slices containing LHb were cut using a Leica VT1000s or VT1200 vibratome. Following cutting, each slice was recovered for 9–11 min individually in a pre-warmed (34°C) choline-based solution containing (in mM) 110 choline chloride, 11.6 ascorbic acid, 3.1 pyruvic acid, 2.5 KCl, 25 $NaHCO_3$, 1.25 NaH_2PO_4, 0.5 $CaCl_2$, 7 $MgCl_2$, and 25 glucose, then for at least 20 min in a secondary recovery chamber filled with 34°C aCSF. After recovery, the slices in aCSF were cooled down to and maintained at room temperature until use. Choline and aCSF solutions were under constant carbogenation (95% O_2/5% CO_2).

Electrophysiology

For whole-cell recordings, individual slices were transferred to a recording chamber mounted on an upright customized microscope with the DMOS system. LHb neurons were visualized using an infrared differential interference contrast method under a 40× water-immersion Olympus objective. Epifluorescence (LED light source from X-Cite 120Q, Excelitas) was used to confirm virus expression and to identify regions displaying high density of *SSt+ tdTom+* axons within the LHb. Recording pipettes (2–3 MΩ) were pulled from borosilicate glass using P-97 Flaming/Brown type micropipette puller (Sutter). Pipettes were filled with cesium-based internal recordings solution consisting of (in mM) 135 $CsMeSO_3$, 10 HEPES, 1 EGTA, 4 Mg-ATP, 0.3 Na-GTP, 8 Na_2-Phosphocreatine, 3.3 QX-314 (Cl- salt), pH adjusted to 7.3 with CsOH, and diluted to 290–295 mOsm/kg. Whole-cell voltage-clamp recording was performed in acute slices continuously perfused with carbogenated aCSF at room temperature at a flow rate of 3~4 ml/min. After forming an intracellular seal with a target LHb neuron, 473-nm light stimulus was delivered using the full field-of-view of the DMOS setup to activate oChIEF expressing *Sst+* presynaptic axons to confirm a synaptic transmission onto the postsynaptic cell. In LHb neurons that elicited PSCs, we subsequently delivered stimulation pulses (2~5 ms pulse duration, 100-ms interstimulus interval) consisting of 96 patterns of 23 × 28 μm boxes that tiled the entirety of the DMOS field-of-view to identify regions that gave rise to PSCs due to groups of axons. Voltage-clamp recordings were amplified and low-pass filtered at 3 kHz using a Multiclamp700 B (Axon Instruments, Molecular Devices) and digitized at 10 kHz using an acquisition board (National Instruments). Data were saved with a custom version of ScanImage written in MATLAB with the DMOS package that enabled mapping of the electrophysiological recording that contain PSC elicited by photo-stimulation to a spatial coordinate on the sample plane. Using this mapping table, we were able to reconstruct a spatial heatmap indicating the location coordinate of presynaptic axons that synapsed onto the postsynaptic neuron that we recorded from. All recordings were performed with R,S-3-(2-carboxypiperazin-4- yl) propyl-1-phosphonic acid (CPP, 10μM Tocris) in bath solution to block NMDAR-mediated excitatory postsynaptic current. For all experiments, the membrane potentials were left uncorrected for liquid junction potential (empirical = 9.3 mV; theoretical = 10.6 mV).

For the compound PSC recording experiment described in Figure 3, LHb neurons were voltage-clamped at a holding potential of −70 mV, while the DMOS system delivered a light stimulation pattern consisting of a spatiotemporal sequence of 96 different spots for five consecutive sweeps. The cell was subsequently depolarized to a holding potential of 0 mV and delivered the same stimulation pattern for another five consecutive sweeps.

For the minimal stimulation PSC recording experiment described in Figure 4, LHb neurons were voltage-clamped at an intermediate holding potential of −35 or −27 mV, while the DMOS setup delivered light stimulation pattern of 96 different spots in each trial.

Please cite this article in press as: Kim et al., Co-packaging of opposing neurotransmitters in individual synaptic vesicles in the central nervous system, Neuron (2022), https://doi.org/10.1016/j.neuron.2022.01.007

To ensure that we are only targeting presynaptic boutons, tetrodotoxin (TTX, 1 μM Tocris) and 4-Aminopyridine (4-AP, 400 μM Tocris) were present in the bath solution at room temperature (24°C ± 0.5°C) throughout the experiment. Initial five trials collected, using high laser intensity, were used to determine the spatial map of input-output responses in the recorded cell. Next, custom software written in MATLAB was used to select a few hotspots out of the 96 candidate spots to enable rapid collection of hundreds of trials of data at these hotspots. In some occasions, these spots were then subdivided into smaller regions, and the final hotspots widths ranged from 10∼30 μm, depending on our ability to evoke a PSC after reducing the stimulation spot size. After finalizing a stimulation pattern, we then manually adjusted the laser intensity using the Laser Quantum RemoteApp software until some of these spots elicited PSCs stochastically upon repetitive stimulation.

For the serotonin, 2-chloroadenosine, and CP93129 bath application experiment with DMD ring illumination (Figures 7A, 7B, and S8A–S8C), LHb neuron voltage-clamp recordings were performed at holding potentials of −64 and 10 mV, in the presence of CB_1 receptor antagonist AM251 (1 μM, Tocris) at physiological bath temperature (34°C ± 0.5°C). 1 μM Serotonin hydrochloride (Tocris), 100 μM 2-chloroadenosine (Tocris), or 1 μM CP93129 hydrochloride (Tocris) was applied to perfusion chamber to compare the effect of serotonin on glutamate/GABA co-release at a macroscopic level. For the serotonin bath application experiment with presynaptic terminal stimulation (Figures 7C–7L), the same experimental condition as in Figure 4 was used with 0.25 μM serotonin hydrochloride (Tocris) to reduce synaptic release probability. For the 2-chloroadenosine bath application experiment with presynaptic terminal stimulation (Figure 8), the same experimental condition as in Figure 4 was used with 100 μM 2-chloroadenosine (Tocris) to reduce synaptic release probability.

Model simulations

We developed a biophysical model simulating a probabilistic neurotransmitter release with small variance in the vesicle content. To simulate excitatory and inhibitory postsynaptic currents due to a single vesicle release, we used the *alpha function* of the form:

$$I(t) = u(t)\frac{I_{max}}{\tau}\left(te^{1-\frac{t}{\tau}}\right) \quad \text{(Equation 2)}$$

where τ is the time constant determining on- and off-kinetics of the function (τ_E=1ms and τ_I=3ms were used for excitatory and inhibitory PSCs, respectively), I_{max} is the maximum amplitude of the current change, and $u(t)$ is a unit step function that represents the onset of vesicle release. In the co-packaging version of the model, the excitatory and inhibitory PSCs occurred together, and the vesicle noise was shared. In the independent version, the two PSCs occurred independently from each other with independent vesicle noise. The currents mediated by two different neurotransmitters were summed to generate net currents of two versions of release model:

$$I_{co-packaging}(t) = a_i I_E(t) + a_i I_I(t) + \xi(t) \quad \text{(Equation 3)}$$

$$I_{independent}(t) = a_i I_E(t) + b_i I_I(t) + \xi(t) \quad \text{(Equation 4)}$$

where $\xi(t)$ is the white noise with standard deviation $\sigma = 0.05$, which scales with the signal size. a_i and b_i represent the scaling factor of the single vesicle content of the i^{th} trial

$$a_i \sim N(1, \sigma_{vesicle}) \quad \text{(Equation 5)}$$

$$b_i \sim N(1, \sigma_{vesicle}) \quad \text{(Equation 6)}$$

where $\sigma_{vesicle}$ is the standard deviation of fluctuations in the vesicle content across trials. We simulated 200 trials to generate a distribution of net currents using the same parameters for the 2 versions of model in MATLAB (available from https://github.com/seulah-kim/coreleaseAnalysis_Kim2021).

Analysis of electrophysiology data

All analysis steps were performed in MATLAB (available from Github: https://github.com/seulah-kim/coreleaseAnalysis_Kim2021). Schematic of analysis pipeline is shown in Figure S4A.

Quality check

To ensure that we only include data collected with stable recording and that observed changes in evoked current peak size across trials are not due to variable amount of filtering because of fluctuations in resistance, access resistance between the pipette and the target cell was computed for every trial by fitting an RC response curve with two exponential functions and extrapolating the instantaneous peak size. The estimated access resistances across trials were median filtered, using window size of 2 ms, to identify trials that exceeded 25% percentage of the initial access resistance, which was estimated from a median value of the first third trials of the total data recorded. In addition, we eliminated trials with >30 pA drift in voltage-clamp recording within the trial. Across trials, any outliers that exceeded 30 pA from the median of average trial value were eliminated.

Pre-processing

Raw current signals were baseline subtracted using the mean of baseline period (299.9 ms) of each trial. The offset signal was then low-pass filtered at 2 kHz and smoothed using a savitsky-golay filter with polynomial order of 5 and frame length of 2.7 ms, followed

Please cite this article in press as: Kim et al., Co-packaging of opposing neurotransmitters in individual synaptic vesicles in the central nervous system, Neuron (2022), https://doi.org/10.1016/j.neuron.2022.01.007

by a moving median filter of 0.6 ms window. The current traces of all trials were grouped based on the stimulation location and then aligned with respect to the light onset of individual spots. Each trial was subsequently baseline offset based on the average current of the stimulation period.

Identification of putative hotspots and changepoint analysis

Median absolute deviation of individual time point was calculated across trials, for individual spots. If a spot contained time points that exceeded the 3 scaled median absolute deviation away from the median value for longer than five consecutive milliseconds, it was sorted as a hotspot. The rest of spots that did not meet these criteria were sorted as null spots. To determine the time window for trial-by-trial statistical analysis, changepoint analysis was performed on the light onset aligned traces of hotspots. This method identified an onset and an offset of evoked response time window such that the sum of the residual error of the three partitioned regions is minimized in the local root mean square level.

Fitting a noise model for individual cells

Null spots and 30-ms period prior to photo-stimulation onset data were pooled to fit a gaussian distribution noise model for individual cells and extract standard deviation of the symmetric noise centered around the baseline current recording of each cell.

Maximum/minimum amplitude extraction and trial classification

To extract maximum and minimum amplitudes described in Figure 5, hotspots traces (time × trials) were further divided into pre-stim (−30 to 0 ms, relative to light-onset) and evoked periods. Maximum and minimum peak locations were identified trial-by-trial per hotspot for individual periods. Amplitudes of maximum and minimum peaks during evoked period were estimated by computing 1 ms average around the initial peak locations and subtracting the average value of the time window spanning −13 to −3 ms, prior to the individual peaks as baselines. Same steps were repeated using the pre-stim period data to create the null distribution of maximum and minimum amplitudes. Trials with either the maximum or minimum amplitude that was greater than 2 scaled standard deviation of symmetric noise of a given cell were classified as success. The rest of the trials were classified as failures.

Classification of hotspots and subtypes

To determine the final list of hotspots, we bootstrapped maximum and minimum amplitude pairs extracted from the pre-stim periods of individual hotspots 10,000 times to generate null distributions of probability of excitatory (p(E)), inhibitory (p(I)), and both ($p \cap I$) PSCs, using the same criteria defined above for classifying trials as presence or absence of events. This was to account for spontaneous activity rate that would give rise to success rate observed during pre-stim period, and we wanted to ask whether observed success rate during the evoked period was statistically significant compared with the null success rate of pre-stim period.

Furthermore, we categorized individual hotspots into EPSC-only, IPSC-only, and both subtypes, described in Figure 4. In EPSC-only hotspots, only the p(E) during evoked period exceeded the 95% confidence interval of the bootstrapped null distribution of p(E). In IPSC-only hotspots, only the p(I) of evoked period exceeded the 95% confidence interval of the bootstrapped null distribution of p(I). In both hotspots, both p(E) and p(I) of evoked period exceeded 95% confidence interval of the bootstrapped null distributions of p(E) and p(I), respectively.

DMOS spatial heatmaps

Total charge of PSC was measured in a 5–25 ms time window after the onset of photo-stimulation.

3 Statistical features

Probability feature determines the presence or absence of the EPSC and IPSC on each trial but does not consider amplitudes of the detected currents. The occurrence of two events (e.g., detecting an EPSC or an IPSC) are statistically independent if and only if the probability of the events occurring together, or the joint probability, is equal to the product of the probabilities of each occurring. We adopted this framework to test if the observed probabilities of occurrence of PSCs with EPSCs, IPSCs, or both are consistent with the results predicted by statistical independence.

Cdf feature examines if the minimum PSC amplitude distributions are the same whether or not an IPSC was detected in the trial (“I” or “no I” trials, respectively). The converse – the PSC maximum amplitude distributions for EPSC and no EPSC containing trials (“E” or “no E trials”, respectively) – was also examined. In fact, the requirement of judging the presence or absence of either component can be relaxed, and the same analysis can be performed by simply dividing the PSC into those with, for example, large and small amplitude IPSCs and asking if this influences the distribution of EPSC amplitudes (Figure S2A). The relaxed requirement still produces distinguishable differences between the two models, demonstrating that, even if signal-to-noise (SNR) of recordings is low, this statistical test is robust.

Correlation analysis was performed separately for all trials and for success trials to account for possible analysis artifacts resulting from inclusion of noisy failure trials. In the independent release model, the distributions of the correlations between maximum and minimum PSC amplitudes are consistently negative when calculated for all trials and for success trials (Figure 2F). The negative correlation is explained by the fact that a large (compared with the mean) EPSC reduces the peak of an independently generated (and therefore, on average, mean amplitude) IPSC and vice versa. In contrast, simulation of the co-packaging model produces strong positive correlations (essentially 1) for all trials and for success trials (Figure 2F). This high correlation results from (1) co-occurrence of successes and failures in EPSCs/IPSCs and (2) shared variance due to vesicle-to-vesicle size differences, which co-modulates the two opposing currents. In each case, null correlation distributions were computed by shuffling the maximum and minimum

Please cite this article in press as: Kim et al., Co-packaging of opposing neurotransmitters in individual synaptic vesicles in the central nervous system, Neuron (2022), https://doi.org/10.1016/j.neuron.2022.01.007

amplitudes across trials and, as expected, are centered at zero in both models (Figure 2F). This assay, when applied to all trials, does not require judging the presence or absence of either the EPSC or IPSC in each trial.

Simulations of biophysical models using the experimental PSC parameters were performed n = 500 runs.

Parametrization of model feature indicator

Model feature indicator derived from probability feature was computed by subtracting the probability value for which cdf = 0.5 of p(E)*p(I) distribution (gray) from that of p(E ∩ I) distribution (purple) (Figures 5C, 5H, and 6A). $\Delta cdf_{0.5}$ captures the direction and magnitude of the relative shift of the feature distribution compared to the null.

For i_{min} feature output, model feature indicator was calculated as a difference in normalized minimum amplitude, i, for which cdf = 0.5 between the groups with presence (solid red) and absence (dashed red) of an inhibitory current (Figures 5D and 5I). Similar analyses were performed for i_{max} feature output for maximum amplitudes between groups with presence (solid blue) and absence (dashed blue) of an excitatory current. Model feature indicators for $correlation_{all}$ and $correlation_{s}$ outputs were calculated as the difference in correlation value for which cdf = 0.5 between all trials (dark green) and shuffled (gray) and success only trials (light green) and shuffled (gray) groups, respectively (Figures 5E and 5J). For transformation of model feature indicator shown in Figure 6C , probability feature values less than 0 were assigned to zero and then normalized by 0.25, which is the theoretical maximum difference if p(E) and p(I) were assumed to be the same. Correlation features ($correlation_{all}$ and $correlation_{s}$) and cdf features (i_{min} and i_{max}) values were cut off at 0 (floor) and 1 (ceiling). To reduce dimension after parametrization and transformation, we projected each spot on the model axis as the average of five model feature indicators (Figure 6D).

Three types of noise metrics

Symmetric baseline recording noise was computed by fitting a gaussian function (mean and standard deviation) on pooled data consisting of portion of traces that are null spots (Figure S4A) and 300-ms baseline period across trials. Spontaneous activity peaks were extracted using the same method of minimum and maximum amplitude, as described above, applied to 30 ms prior to photostimulation onset on each trial. As a reflection of both the rate and duration of the spontaneous synaptic events, outlier fraction was calculated as the fraction of datapoints exceeding 3 scaled median absolute deviation from the pooled data consisting of null spots and 300-ms baseline period.

SNR of i_{min} and i_{max} were calculated by comparing i_{min} and i_{max} with the EPSC/IPSC detection threshold limited by the baseline current noise.

Analysis of 5-HT pharmacological effect

K-S test was performed with bootstrapping (10,000 times) with resampling size matching the smaller number of trials of the two groups (normally this is post 5-HT group size) to compare before and after 5-HT on the minimum and maximum amplitudes.

i_{min} and i_{max} subset distributions analysis (Figures 7M, 7N, and S7D1–S7D6) was performed by aligning individual trials by the i_{min} time point within the time window determined by changepoint analysis. Trials were sorted in ascending order based on the i_{min} size and then grouped in 10 trials. Maximum and minimum amplitudes were extracted from the average trace of each group aligned by i_{min} peak location.

To specifically test if the correlation between glutamate and GABA receptor currents was maintained after 5-HT application as predicted for the co-packaging model, we developed an alternative test that uses paired data from the basal and drug condition but does not require sorting trials into successes and failures. We compared the distribution of i_{min} and i_{max} amplitudes in trials sorted and binned by i_{min} amplitude—i.e., the 5 trials with largest i_{min} in group 1, the next 5 largest in group 2, etc. A positive correlation of the binned distributions of i_{min} and i_{max} confirmed that these sites were consistent with the co-packaging model (Pearson correlation coefficient = 0.893 [before], 0.817 [after]; $p < 0.001$ [before and after]) (Figures 7M and S7E). Co-packaging versus independent release models make different predictions of the effect of 5-HT on this relationship. In the former, assuming no change in synaptic potency, the range of the data and slope of the relationship showed remain unchanged; indeed, this was the effect observed in the example site (Figure 7M). If there is an additional change in synaptic potency, the relationship should scale along the diagonal, whereas if the effects are differential on glutamate and GABA receptors, the relationship should change slope. In contrast, in an independent release model in which the pre-5-HT consistency with co-packing arose by chance, the relationship should be randomized after 5-HT or possibly reveal a negative correlation reflecting the mutual overlap of excitatory and inhibitory synaptic currents (Figure 7N).

Overall, we found that, after 5-HT application, the binned i_{min} versus i_{max} distribution maintained the correlation slope in three out of six spots (Figures S7E1, S7E4, and S7E6). In the remaining the three spots, a correlation was maintained but the data shifted, consistent with a larger effect on the i_{max} (i.e., IPSC amplitude) distribution (Figures S7E2, S7E3, and S7E5). Such effects could arise from a larger effect on potency of GABAergic versus glutamatergic currents or reflect AMPA receptor saturation in the larger excitatory currents.

For the prediction of model feature indicator change (Figure 7Q), the trials of pre 5-HT condition was analyzed with gaussian noise added to match the post 5-HT condition, subset of success trials were included to match the release probability of post 5-HT condition, and the i_{min} and i_{max} amplitudes of "both" success trials were scaled to match the scaling of pre versus post 5-HT condition of median amplitudes of success trials.

Please cite this article in press as: Kim et al., Co-packaging of opposing neurotransmitters in individual synaptic vesicles in the central nervous system, Neuron (2022), https://doi.org/10.1016/j.neuron.2022.01.007

Technical concerns involving our study of glutamate/GABA co-release

The success of our analysis method depends on the SNR of the recording and the ability of the algorithm to detect glutamate- or GABA-mediated currents with differing kinetics and amplitudes (Figure S6). The performance of the algorithms and the power of the models depend on the EPSC/IPSC transmission ratio and receptor kinetics and degrade with increasing spontaneous synaptic activity, baseline holding current noise, electronic noise, and numbers of active terminals within each optogenetic stimulation spot. These factors tend to make co-packaging synapses appear as independent synapses. Indeed, our study finds that the likelihood of individual unitary response hotspots being categorized as corresponding to a co-packaging synapse is anticorrelated with level of spontaneous PSCs and correlated with average EPSC/IPSC SNR of the synapse (Figures 6E–6G).

In this study, the ability to detect glutamate and GABA release depends on the expression of ionotropic receptors for each transmitter in the postsynaptic terminal associated with the stimulated bouton. Therefore, we are unable to state whether synapses in which we observe only glutamate- or only GABA-mediated currents reflect terminals that release only one transmitter or postsynaptic terminals that are exposed to both transmitters but lack one of the receptor classes. Furthermore, given the small size of unitary synaptic currents and the ability of excitatory and inhibitory currents to obscure each other, in some glutamate-only or GABA-only spots it is possible that the missing current was simply hidden.

A possible source of error that could make independent sites appear as co-packaging sites is large variability in stimulation intensity that drives the correlation of amplitudes observed across trials. In this case, the stimulation intensity would have to vary sufficiently to stochastically excite one or a small set of synapses that independently release glutamate and GABA, but do so with probability of release near 1. However, online measurements of the DMOS photo-stimulation intensity demonstrate that trial-to-trial variations in stimulation intensity are small (<1%) and uncorrelated with the categorization of each trial as success or the amplitude of the EPSC and IPSC in a given trial (Figure S5B).

QUANTIFICATION AND STATISTICAL ANALYSIS

Comparisons of proportions of hotspots were done using Fisher's exact test. Formal tests were not used to assess data distributions. Bootstrapping (10,000 times) method was used to simulate variance in the sampling for statistical tests. Lower boundary of p value for bootstrapped results was set by the bootstrap number (e.g., $p = 1/10{,}000 = 0.0001$). Cumulative distributions were compared using Kolmogorov-Smirnov tests.

Graphs were generated with custom-written scripts in MATLAB. The figures were assembled in Illustrator (Adobe). The detailed statistics for all experiments can be found in the respective results and methods sections and figure legends. p Values smaller than 0.001 were reported as $p < 0.001$. The following code was used for p values in the figures: n.s. not significant; * <0.05.

Neuron, Volume *110*

Supplemental information

Co-packaging of opposing neurotransmitters in individual synaptic vesicles in the central nervous system

SeulAh Kim, Michael L. Wallace, Mahmoud El-Rifai, Alexa R. Knudsen, and Bernardo L. Sabatini

Supplemental Figure 1.

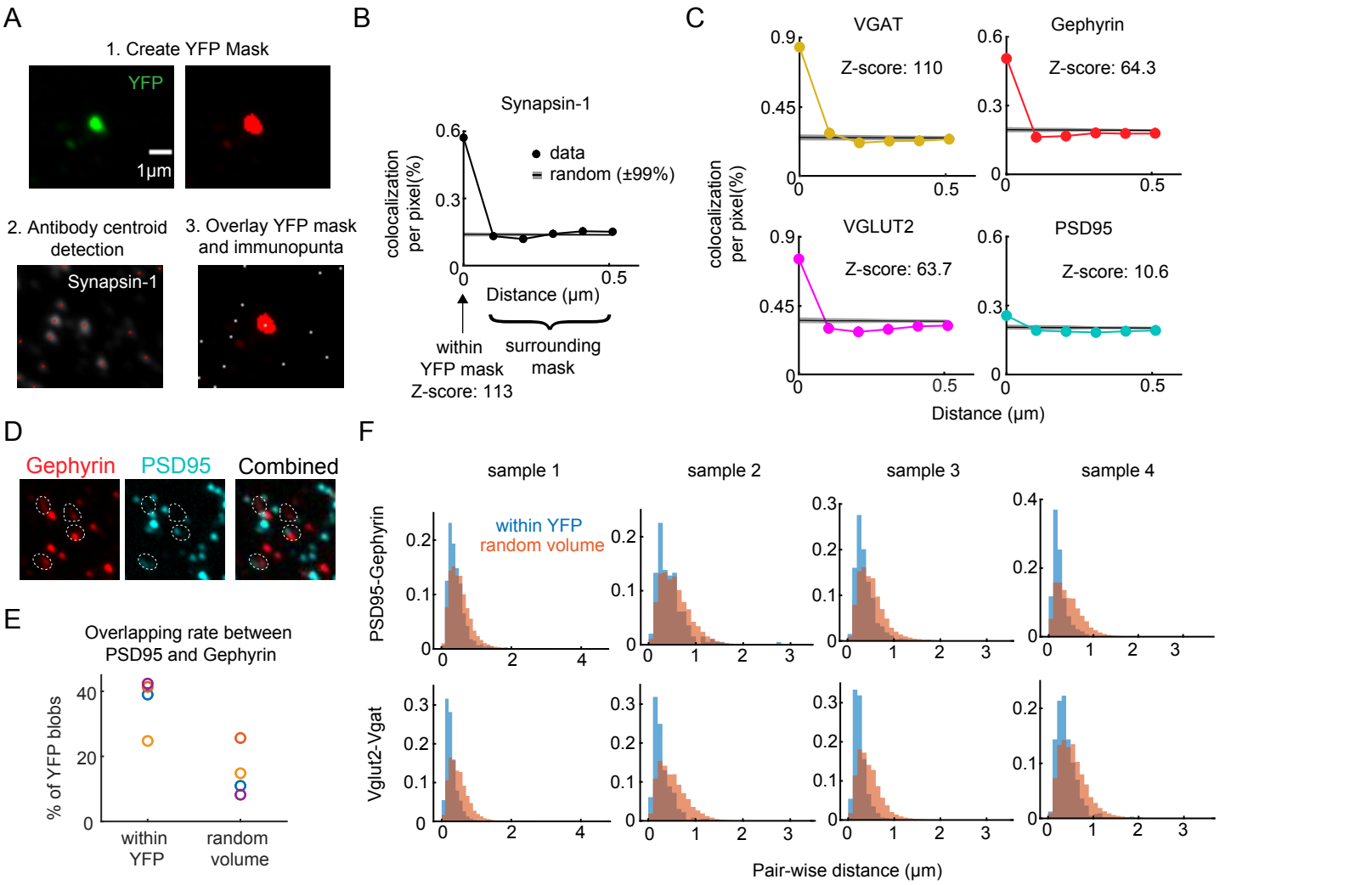

Supplemental Figure 2.

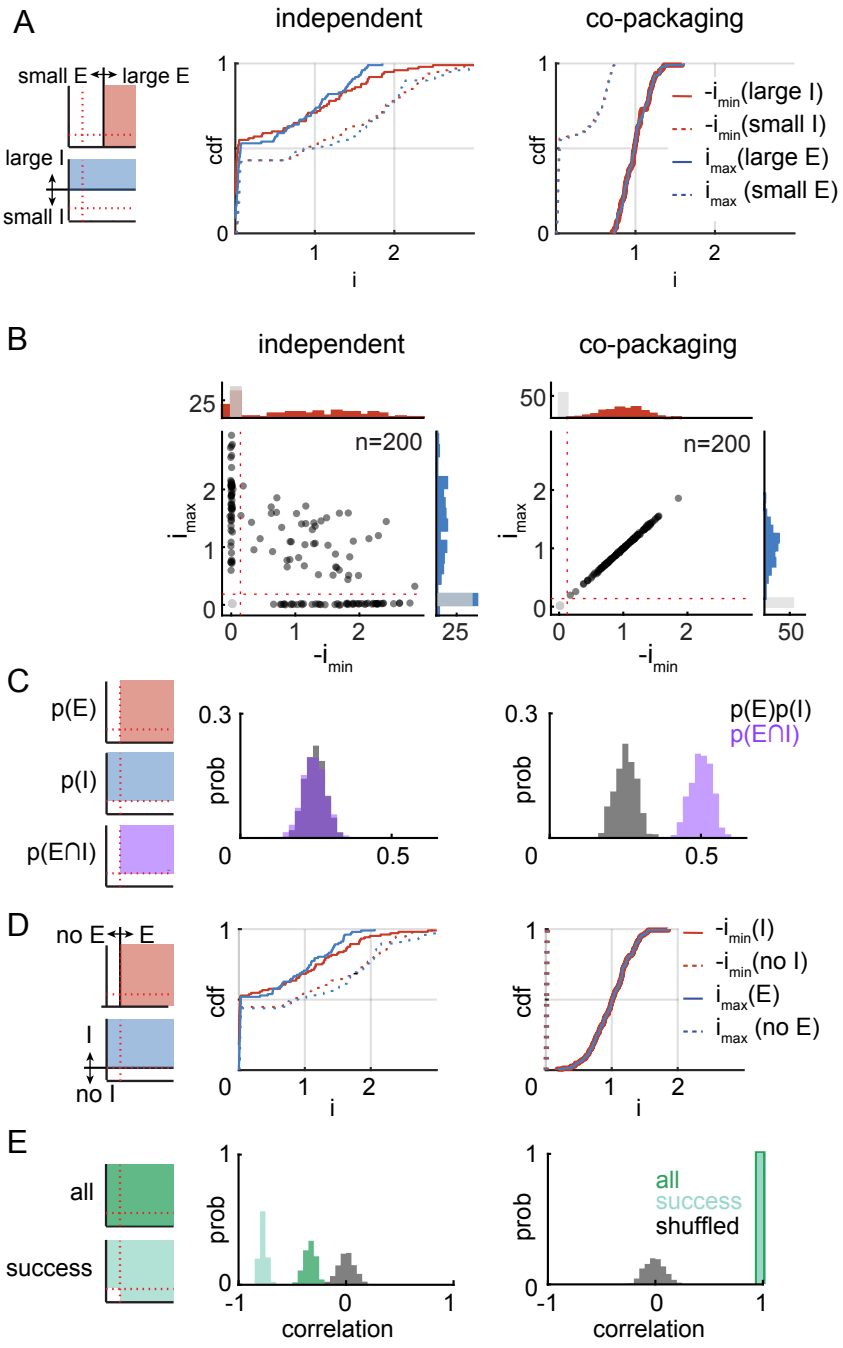

Supplemental Figure 3.

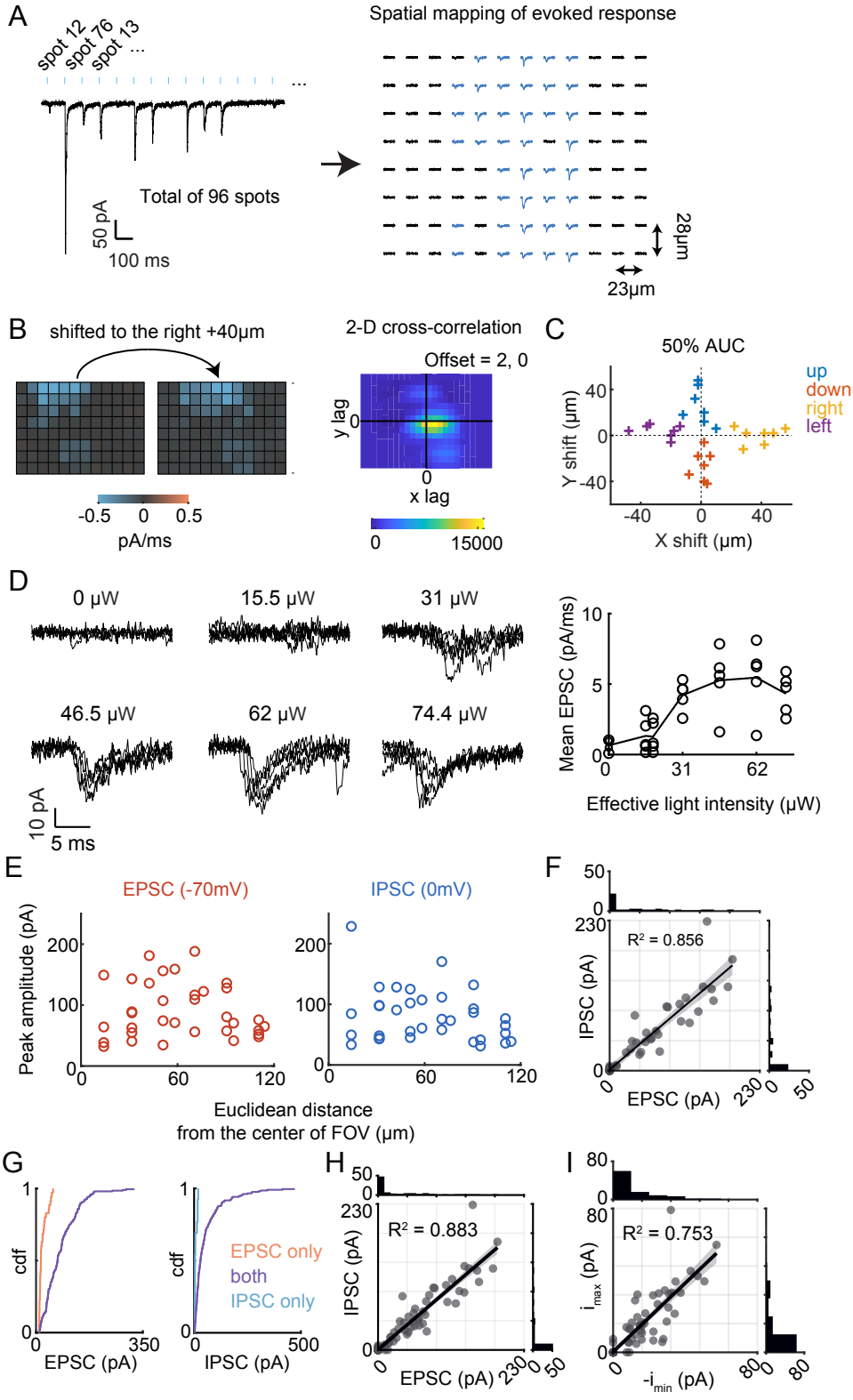

Supplemental Figure 4.

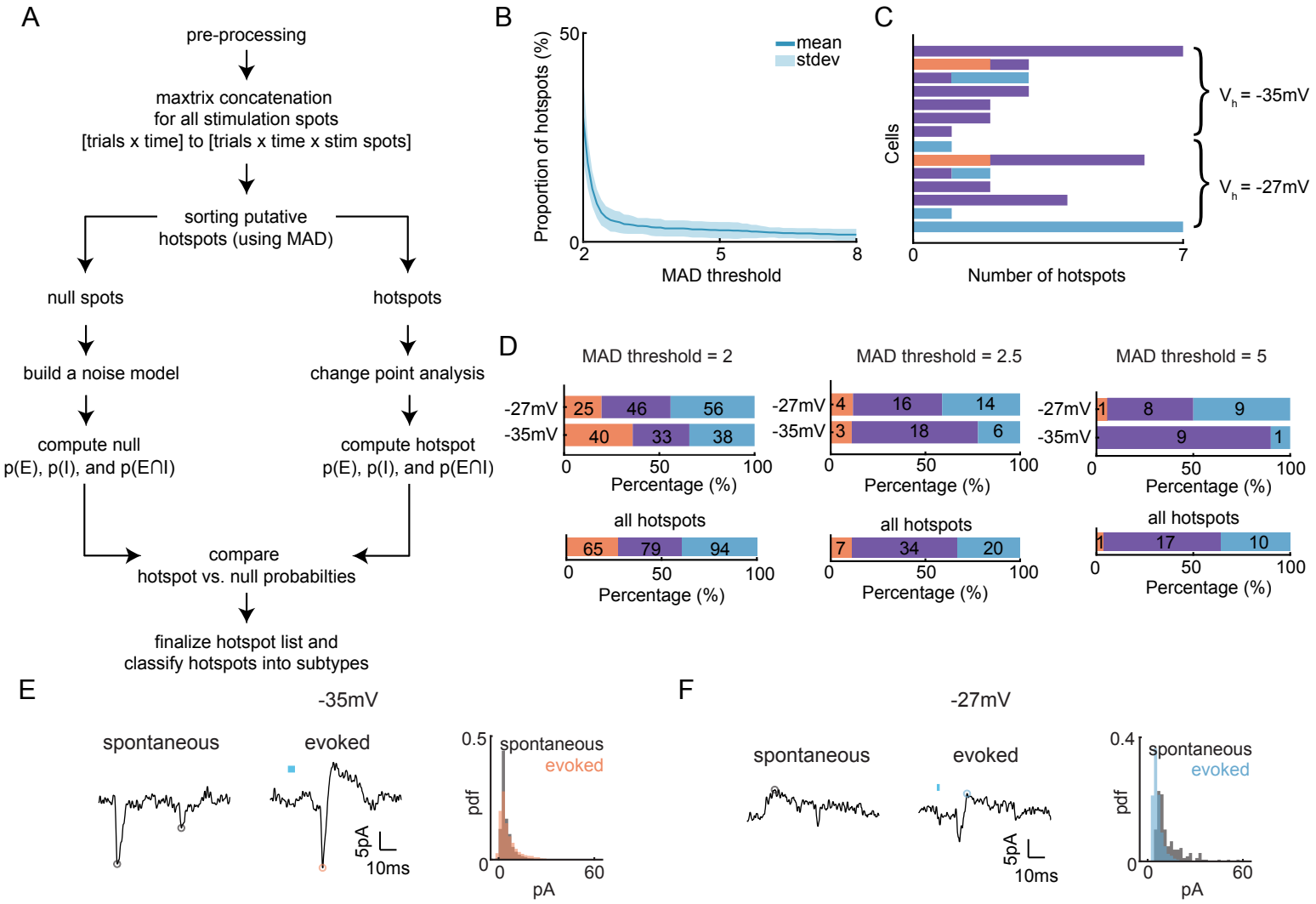

Supplemental Figure 5.

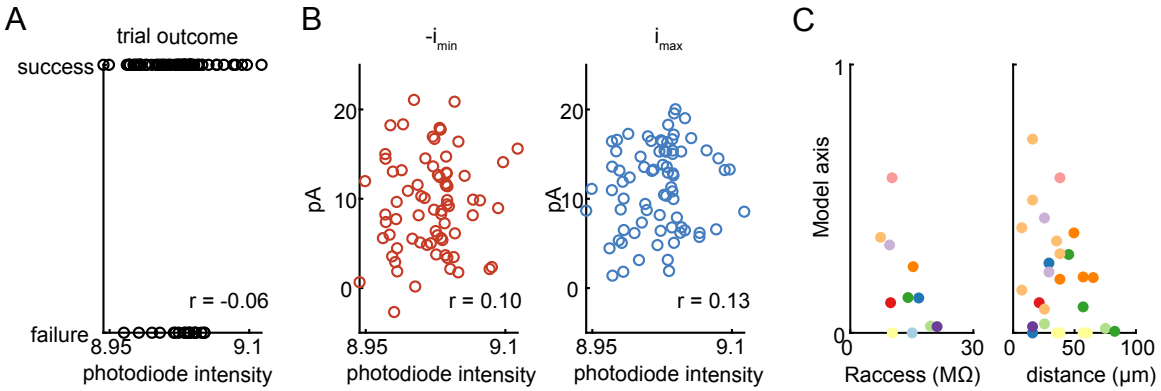

Supplemental Figure 6.

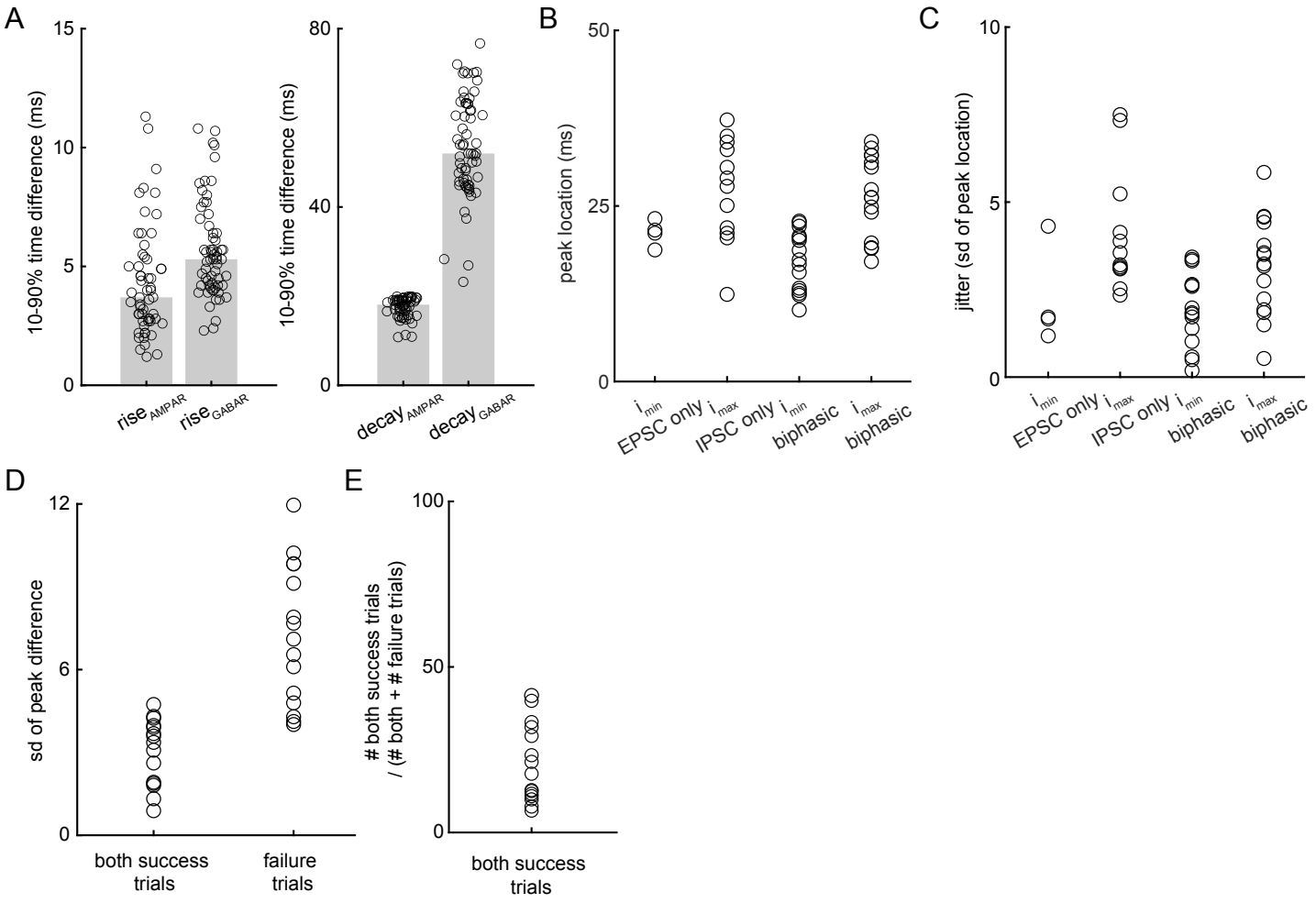

Supplemental Figure 7.

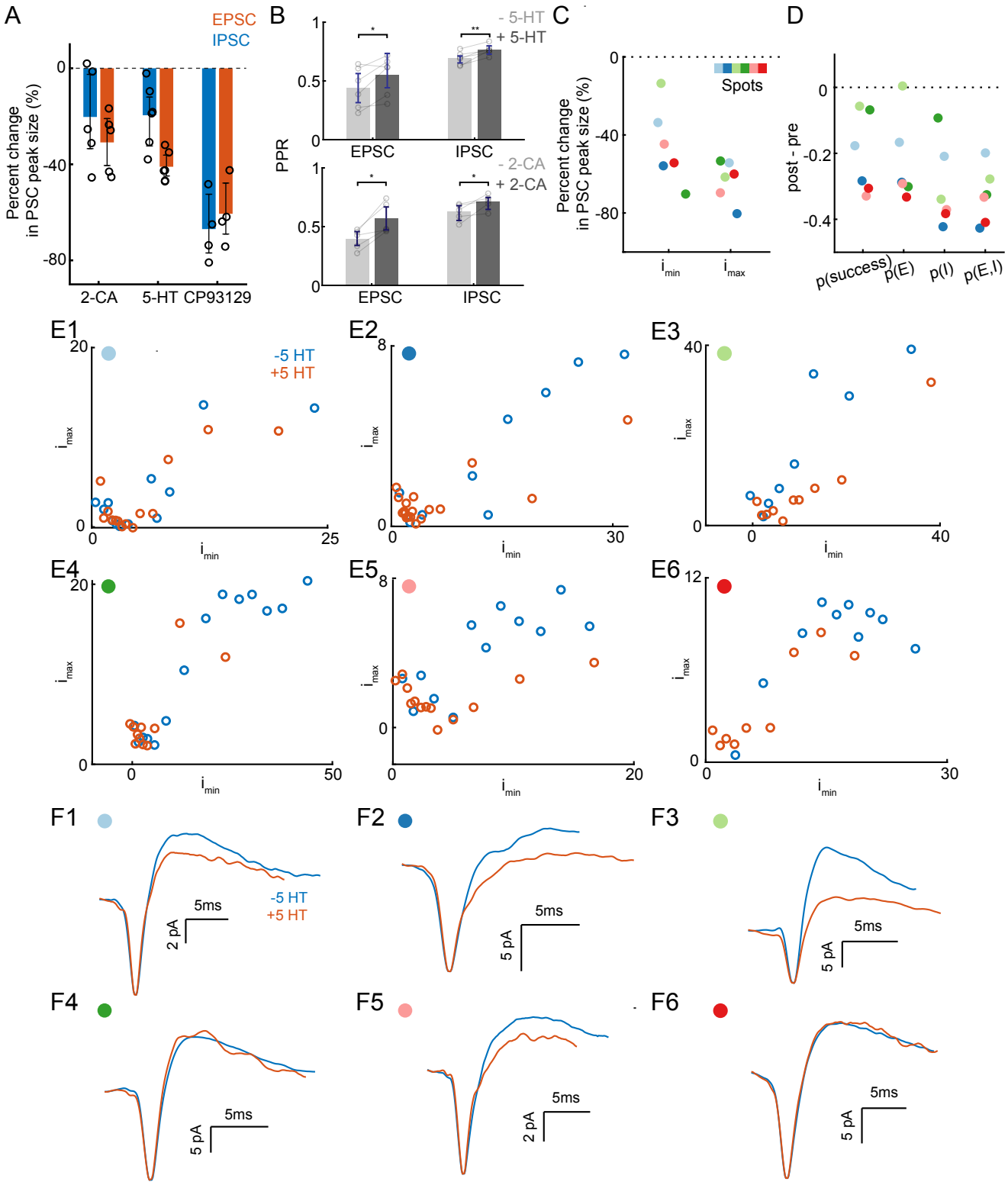

Supplemental Figure 8.

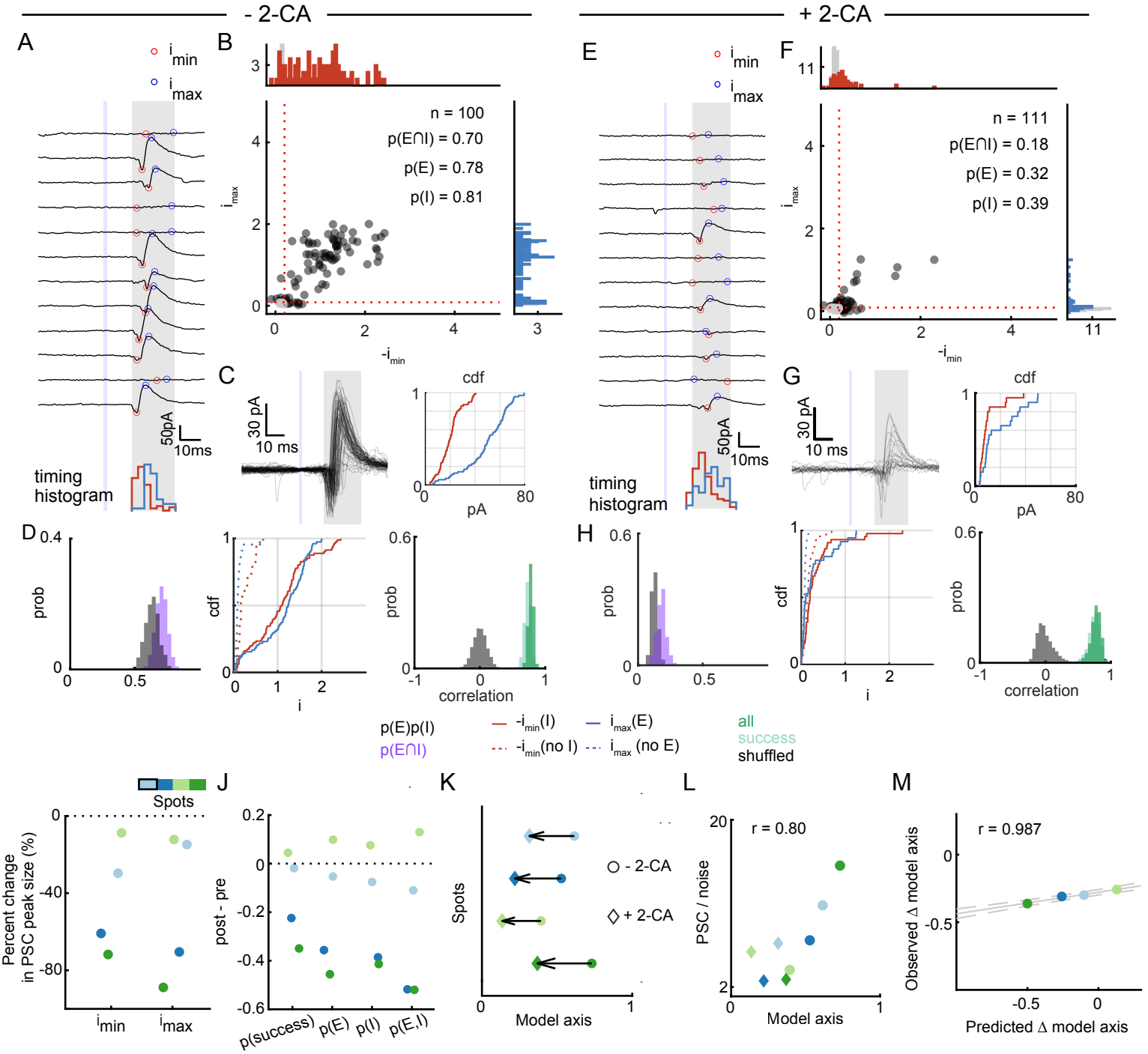

SFig. Legends

SFig. 1. Co-localization analysis of antibodies within and outside of YFP-labelled EP Sst+ terminals. Related to Fig. 1

A) Co-localization analysis schematic. The YFP channel fluorescence was used to create masks to identify pixel regions containing labeled *Sst+* terminals. Each antibody channels was analyzed independently to extract the locations of the centroids of immunolabeled puncta. Extracted centroid locations were compared to the YFP masks in the same sample plane. For each immunolabeling channel, the percentage of pixels in the YFP+ masks that contained a punctum centroid was calculated and is referred to as the "co-localization" metric.

B) Example synapsin-1 immunopuncta co-localization within the YFP mask and the surrounding regions compared to that expected by chance. Antibody locations were randomized 1000 times and the 99th percentile upper and lower boundaries are shown. Z-score is calculated as the difference between the mean antibody co-localization within the YFP mask and the mean randomized co-localization, divided by the standard deviation of the random co-localization.

C) Example co-localization analysis results for Vgat, Gephyrin, Vglut2, and PSD95 antibodies from the tissue sample shown in B.

D) Enlarged images of the inset in Fig 1C demonstrating colocalization in YFP-labelled *Sst+* terminals and the postsynaptic proteins for scaffolding of GABA (Gephyrin) and glutamate (PSD95) ionotropic receptors.

E) Overlapping rate of Gephyrin and PSD95 immunopuncta inside the same YFP blobs compared to a random volume of similar area size.

F) Paired distances between Gephyrin-PSD95 (top) and Vglut2-Vgat (bottom) puncta pairs within YFP volumes and random volumes.

SFig. 2. Accurate separation of synaptic failures is not required for the cdf analysis. Related to Fig. 2

A) Simulated cdfs of maximum PSC amplitudes (i_{max}, blue) given a large (i_{max}(E), solid) or small (i_{max}(no E), dashed) excitatory current in the same trial for the independent (*left*) and co-packaging (*right*) release models. Similar analyses were performed for the minimum PSC

amplitudes ($-i_{min}$, red) given large ($-i_{min}(I)$, solid) or small ($-i_{min}$(no I), dashed) inhibitory currents in the same trial. Simulation parameters are the same as in Fig 2D. Here we used the median to separate currents into large and small.

B-E) Simulation results as in Fig. 2C-F with colored noise (3kHz corner frequency Bessel filtered).

SFig. 3. DMD based photo-stimulation enables spatially-specific activation of EP *Sst+* OChIEF-expressing terminals. Related to Fig. 3

A) *left*, Each trial consisted of rapid serial illumination of 23 x 28 µm photo stimulation spots to 96 different locations tiling the field of view in a pseudorandom spatial pattern such that the PSCs evoked from each spot are recorded in ~10s voltage-clamp trace. Shown here is an example recording at -70 mV. *right,* The 96 PSCs in each trace are extracted and assigned to spatial locations based on the coordinates of the illuminated spots and the stimulus timing.

B) Example showing that the DMD-evoked spatial map is consistent with the physical locations of EP *Sst+* terminals. *left,* the input-output relationship was initially mapped (V_h=-70mV) using the DMD-based optogenetic stimulation platform then the brain slice was shifted in +x direction relative to the microscope objective lens by 40 µm after which the input-output relationship was re-mapped. *right*, 2D cross-correlation of the two spatial maps (before and after the objective lens movement) reveals that the two images are offset by 2 pixels, as predicted by the pixel spacing. The offset is calculated from the X and Y locations where the cumulative sums of correlation coefficient across y and x, respectively, reach the 50% of the total sum. Spatial maps are calculated from the average of 5 trials.

C) Summary of quantification of cross-correlation calculated shifts as described in (B) for 7 cells from 3 animals. Colors indicate the direction of the slice movement.

D) Saturation of the amplitude of the evoked PSC from the same 23 x 28 µm photo-stimulation spot in an example LHb neuron. *left,* electrophysiological recording (V_h=-70 mV) for 5 trials at each indicated light intensity. Traces correspond to 5-25 ms time window after stimulation onset. *right,* Individual (circle) and average (line) EPSC amplitudes as a function of illumination intensity.

E) Relationship between distance of the stimulation spots from the LHb cell body (located at the center of field of view (FOV)) and the corresponding evoked EPSC (*left*) and IPSC (*right*) peak amplitudes (data shown for the same neuron as in Fig 3F).

F) Scatterplot of IPSC vs. EPSC peak amplitude pairs evoked at photo-stimulated spots within 80 µm perimeter from the center of the field of view from the neuron analyzed in Fig 3F.

G) Cdfs comparing the EPSC and IPSC amplitude distributions in different classes of hotspots. EPSC-only (*left,* orange) and IPSC-only (*right*, blue) hotspots have smaller amplitudes than do co-transmission hotspots (purple).

H) Scatterplot of IPSC vs. EPSC amplitudes evoked at each spot for an example LHb neuron. The IPSC/EPSC amplitude ratio is conserved across multiple sets of EP *Sst+* axons synapsing onto the same postsynaptic cell. The top and right histograms show the distributions of EPSC and IPSC amplitudes, respectively. Fitted line: $y = 0.438 + 0.856x$.

I) Scatterplot of i_{max} and i_{min} at V_h=-35 mV for the trace shown in Fig 3E. The top and right histograms show the distributions of $-i_{min}$ and i_{max}, respectively. Fitted line: $y = 0.316 + 0.955x$.

SFig. 4. Automated analysis of evoked unitary responses. Related to Fig. 4

A) Hotspot detection and classification analysis pipeline flowchart (see Methods).

B) Effect of median absolute deviation (MAD) threshold on the proportion of putative hotspots out of total stimulation spots. The MAD threshold, expressed in multiples of the empirically measured MAD for each cell, determines the selection of putative active hotspots which are required to have current deviation that exceed the threshold at least 5ms (the branching step in panel A). Mean and standard deviation of the proportion of illuminated spots designated as hotspots (data from 14 cells are shown). A MAD threshold of 3 was used for Fig. 4F.

C) Distribution of putative hotspot numbers across all cells (n=14 cells, 9 animals). MAD threshold of 3 was used. The holding potential of individual cells is indicated. PSCs are designated as EPSCs only (red), IPSCs only (blue), or both (purple).

D) Effect of MAD threshold on the proportion of final hotspot subtypes. As in Fig. 4F for MAD threshold of 2 (*left*), 2.5 (*middle*), and 5 (*right*). Color code as in (C).

E) Spontaneous EPSCs (*left*) and unitary evoked biphasic PSC (*middle*) recorded from the same cell with evoked EPSC amplitude indicated. *right*, Histograms of amplitudes of spontaneous EPSCs (gray, median amplitude 95% CI=3.37-3.50 pA, median frequency=8.9 Hz; 14 cells, 9 animals) and evoked EPSCs measured in a subset of cells with unitary biphasic PSCs (orange, median amplitude 95% CI=3.82-4.17 pA; 11 cells, 6 animals).

F) As in panel E for a spontaneous and unitary evoked IPSCs. The spontaneous IPSCs (gray) had median amplitude 95% CI=9.15-10.51 pA and frequency=0.2 Hz whereas the evoked IPSCs (blue) had median amplitude 95% CI =3.84-4.18 pA.

SFig. 5. Control analyses for unitary biphasic PSCs. Related to Fig. 5

A-B) Stimulation intensity fluctuation as detected by a photodiode versus trial-by-trial outcome (A)amplitudes of $-i_{min}$ and i_{max} (B). Same dataset as in Fig. 5F)-J).

C) Average model feature indicators for individual spots vs. access resistance (*left*) and Euclidean distance of stimulation site from the center of FOV (*right*). Same dataset as in Fig. 6E).

SFig. 6. Receptor kinetics and jitter analysis. Related to Fig. 4

A) Rise (*left*) and decay (*right*) times of the AMPAR- and $GABA_A$R-mediated postsynaptic currents. Recordings in presence of 10 µM CPP at Vh=-64mV and 10mV. Time difference between 10% and 90% of peak was measured for rise and decay of each stimulated spots that evoked PSCs larger than 30pA.

B) Maximum and minimum peak location from the stimulation onset of EPSC only, IPSC only, and both hotspots in Fig. 4F.

C) Jitter of maximum and minimum peaks in EPSC only, IPSC only, and both hotspots from Fig. 4F.

D) Standard deviation of maximum and minimum peaks in both hotspots from Fig. 4F.

E) Proportion of both success trials relative to the total trial number shown in D).

SFig. 7. Activation of serotonin and adenosine receptors affect glutamate/GABA co-release from EP *Sst*+ terminals in LHb. Related to Fig. 7

A) Peak amplitude changes in the DMD ring stimulation evoked composite EPSC (-64 mV) and IPSC (10 mV) as result of 2-CA (100 µM), 5-HT (1 µM), and CP93129 (1 µM). Each circle represents the difference in mean evoked peak amplitude of 15 trials before and after each drug application. Bars and error bars indicate the mean and bootstrapped 95% confidence interval of the mean, respectively.

B) Normalized paired-pulse ratios before and after bath application of 5-HT (*top*) and 2-CA (*bottom*). Bars and error bars indicate the mean and bootstrapped 95% confidence interval of the mean, respectively. Asterisks represent significance level of paired t-test comparing before and after conditions.

C) Average relative minimum and maximum amplitude changes of DMOS-evoked unitary biphasic spots across all trials as result of 5-HT bath application. Colors indicate spot identity consistent as in Fig. 7O.

D) Changes in probabilities of detecting success trials, EPSC, IPSC, and both trials due to 5-HT bath application for DMOS-stimulated unitary biphasic spots. Each dot represents the difference in probabilities calculated from scatterplot of each spot before and after 5-HT. Colors and markers are consistent as in panel C.

E) The effect of 5-HT on subset distributions of minimum and maximum amplitudes of co-packaging sites, without sorting trials by success and failures. Scatter corresponds to the amplitudes of the average trace of different subsets of dataset before (blue) and after (red) 5-HT bath application. Each dot in the top right indicates spot identity consistent as in Fig. 7O.

F) The effect of 5-HT on the average waveform of co-packaging sites, without sorting trials by success and failures. Average of each trial was aligned by the minimum peak location within the analysis time window. Before (blue) and after (red, normalized by the minimum peak amplitude of "before" condition) 5-HT bath application traces are compared. Each dot in the top right indicates spot identity as in Fig. 7O.

SFig. 8. 2-CA reduces p_r of glutamate and GABA while maintaining their co-packaging. Related to Fig. 8

A-D and E-H) As in Fig. 7E-H and I-L for optically-evoked PSCs from a hotspot consistent with the co-packaging model before (A-D) and after (E-H) application of 2-CA (100 µM)

I) Average relative $-i_{min}$ and i_{max} changes across all trials as result of 2-CA application. Colors indicate spot identity.

J) Changes in probabilities of success, EPSC, IPSC, and both trials due to 2-CA application for DMOS-stimulated biphasic spots. Colors as in panel I.

K-M) As in Fig. 8C-E for the 2-CA effects (n=4) on PSCs from hotspots consistent with the co-packaging model before 2-CA application

Supplemental Tables

Supplemental Table 1. Summary of 5-HT effect on six example co-packaging unitary PSC sites, Related to Fig. 7. Spot annotated with * corresponds to Figure7E-L.

spot	Caveats	Sample size of biphasic trials (before/ after)	Proportion of rejecting null (bootstrapped K-S test) "both" success trials	Proportion of rejecting null (bootstrapped K-S test) all success trials	Mean amplitude (in pA)	Model axis value change (post-pre)	PSC / noise change (post-pre)
*		(52/25)	0.5305(E); 0.3076 (I)	0.5992 (E); 0.8139 (I)	before: 13.5 (E), 14.8 (I); after: 10.4 (E), 13.4 (I)	-0.351	-2.024
	p(I) drops to 0.18 after 5-HT and the spontaneous activity makes cdf difference smaller	(47/18)	0.1616(E); 0.1627 (I)	0.9933 (E); 0.9999 (I)	before: 19.6 (E), 6.83 (I); after: 16.7 (E), 6.30 (I)	-0.585	-3.788
	p(E∩I) reduction could be mostly	(41/23)	0.2257(E); 0.2132 (I)	0.5929 (E); 0.9989 (I)	before: 15.2 (E), 30.7 (I);	-0.341	-2.846

	driven by p(I) reduction				after: 19.4(E), 32.7 (I)		
●	Putative co-packaging double synapse (smaller cluster and larger cluster)	(107/49)	0.998 (E); 0.9712 (I)	1 (E); 1 (I)	before: 19.7 (E), 15.1 (I); after: 9.41 (E), 11.0 (I)	-0.383	-5.392
●		(58/18)	0.1575 (E); 0.245 (I)	0.8604 (E); 0.9147 (I)	before: 10.0 (E), 7.62 (I); after: 9.80 (E), 6.67 (I)	-0.282	-1.324
●	Putative multivesicular release site	(83/34)	0.996 (E); 0.5939 (I)	0.9988 (E); 0.9732 (I)	before: 16.4 (E), 10.2 (I); after: 11.4 (E), 8.58 (I)	-0.0224	-3.488